Handbook of Surfaces and Interfaces of Materials

Volume 1

Surface and Interface Phenomena

Edited by

Hari Singh Nalwa, M.Sc., Ph.D.
Stanford Scientific Corporation
Los Angeles, California, USA

Formerly at
Hitachi Research Laboratory
Hitachi Ltd., Ibaraki, Japan

ACADEMIC PRESS

A Harcourt Science and Technology Company

San Diego San Francisco New York Boston London Sydney Tokyo

Chapter 11

CATALYSIS BY SUPPORTED METAL OXIDES

Bert M. Weckhuysen
Departement Anorganische Chemie en Katalyse, Debye Instituut, Universiteit Utrecht, 3508 TC Utrecht, The Netherlands

Israel E. Wachs
Zettlemoyer Center for Surface Studies, Department of Chemical Engineering, Lehigh University, Bethlehem, Pennsylvania, USA

Contents

1. INTRODUCTION

1.1. General Introduction

Catalysts play a crucial role in modern society and in nature. They can be divided into three groups: homogeneous catalysts, biocatalysts, and heterogeneous catalysts (Fig. 1). Biocatalysts include enzymes and immobilized enzymes and cells, whereas homogeneous catalysts can be either acid/base catalysts and transition metal compounds. Heterogeneous catalysts are the most important in the chemical, pharmaceutical, and environmental industries [1, 2]. They are responsible for the production of more than 85% of all bulk chemicals as well as intermediates and fine chemicals, and for the catalytic destruction of environmentally undesirable compounds [3–16]. One can distinguish in this catalyst group bulk catalysts and supported catalysts. Thus, supported metal oxides are only a part of the catalyst market, although many important industrial applications are based on the use of these catalysts. They

Handbook of Surfaces and Interfaces of Materials, edited by H.S. Nalwa
Volume 1: Surface and Interface Pressure

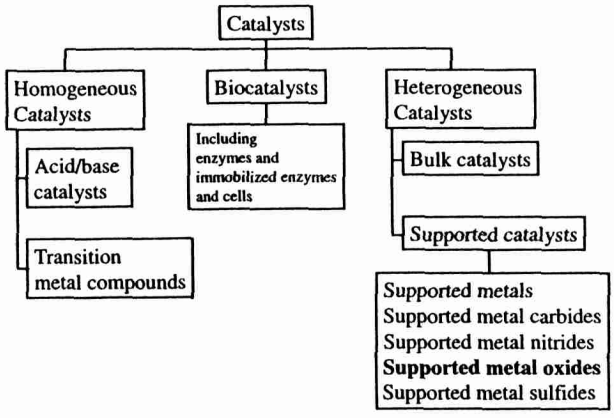

. 1. Overview of the different catalysts existing in nature and society. ›ported metal oxide catalysts are only one type of catalyst used in chemical ustries.

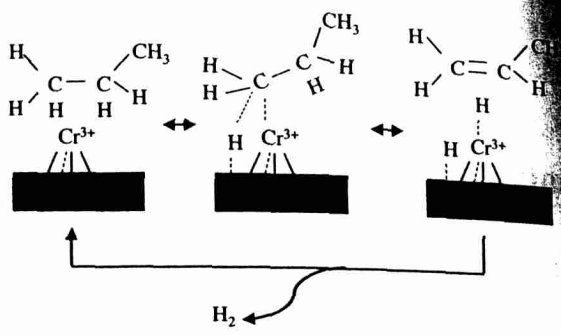

Fig. 2. Possible reaction scheme for the nonoxidative dehydrogenation of alkanes, particularly propane, over supported chromium oxide catalysts. Partially uncoordinated Cr^{3+} species have been detected by spectroscopic techniques in an active alkane dehydrogenation catalyst. (Copyright 1999 Elsevier Science BV.)

nsist of one or more catalytically active metal oxides (e.g., O_5 and CrO_3) dispersed on a support, which is usually a gh-surface oxide, such as SiO_2, Al_2O_3, and zeolites.

The principal properties of supported metal oxide catats are (a) activity (How many molecules are converted by catalytic material per hour?); (b) selectivity (How many the desired molecules are formed by the catalytic mate-l per hour?); and (c) stability (For how many hours, days, nths, or years can the catalytic material do its job in a emical reactor with an acceptable activity and selectivity?). ten chemical promoters (e.g., alkali metal ions) are added optimize these catalytic performances of supported metal ides, whereas structural promoters are added to increase mechanical properties of the catalyst particle. This makes pported metal oxides very complex materials, and this com-xity is even more pronounced for industrially used catalysts cause of the presence of binders, etc. Their study is often volved, and model systems are prepared to reduce their com-xity.

Heterogeneous catalysis starts with the adsorption of a ictant molecule in the gas or liquid phase on the catalytic terial, which is a solid and consists of a (mostly unknown) mber of one or more (also often unknown) catalytically ive sites located on its surface [1, 2]. Adsorption results weakening and eventually breaking of particular chemical nds within this molecule, and the adsorbed species reacts th the surface. This may take place in several fast and con-cutive steps. The chemisorbed species are called reaction ermediates. These species are often undetectable because y are very unstable and therefore only short-lived. Finally, e or more product molecules desorb from the surface into gas or liquid phase. This results in a restructuring of the alyst surface, which again becomes available for the adsorp-n of a new reactant molecule. The function of the cata-t surface is to provide an energetically favorable pathway the chemical reaction. This is made possible by lower-the activation barriers of intermediate steps taking place the catalyst surface in comparison with an uncatalyzed ction.

Figure 2 illustrates a possible reaction scheme for the nonoxidative dehydrogenation of alkanes, particularly of propane [17]. This is an endothermic reaction, which requires a relatively high reaction temperature of 500–600°C. This high reaction temperature can result in side reactions, and a heterogeneous catalyst, such as CrO_3/Al_2O_3, is necessary to obtain economically acceptable yields of alkenes. In a first step, the propane molecule is adsorbed from the gas phase on the catalytic surface, and two C-H bonds within the propane molecule are broken. This process is taking place on an active site, which is assumed to be a reduced Cr^{n+} species. Detailed characterization studies have shown that the active site is most probably a partially uncoordinated Cr^{3+} species [17]. The hydrogen atoms formed, together with the $CH_2CH_2CH_3$ molecule, are bound to the catalyst surface. This adsorbed organic species can be considered as a reaction intermediate, although no one has been able to effectively detect such species. Finally, a propene molecule and a hydrogen molecule are desorbing in the gas phase, and the active sites of the heterogeneous catalyst are regenerated and again available for a new propane molecule in the gas phase. This catalytic cycle can go on until the catalyst material no longer contains active sites. The catalyst is then deactivated.

As heterogeneous catalysis proceeds at the surface of a metal oxide, its surface area has to be as large as possible to have a large number of potentially available active sites. This is accomplished by dispersing the metal oxide phase onto a porous high surface-area oxide. Figure 3 shows an impression of a supported metal oxide catalyst, and Table I gives an overview of some industrially important supported metal oxides and the reaction conditions [2]. The catalytically active metal oxide and the type of high-surface-area support are also included. It is clear that (a) a whole variety of chemical reactions can be catalyzed by these supported metal oxides; (b) the same metal oxide can catalyze totally different chemical reactions, depending on the support composition and type and the reaction conditions; and (c) the same reaction can be catalyzed by different supported metal oxides. These observations already suggest that support materials not only control

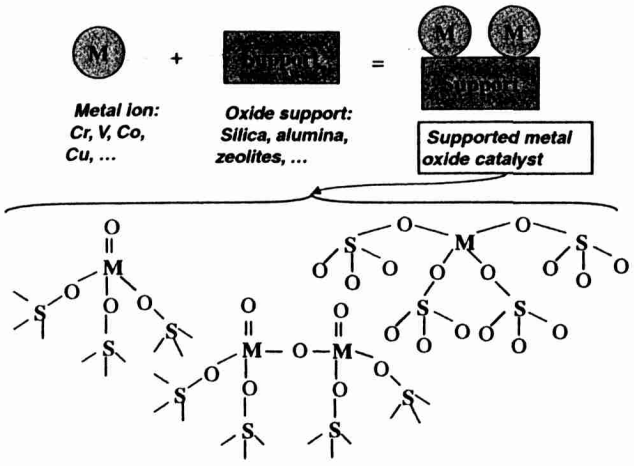

Fig. 3. Schematic representation of supported metal oxide catalysts. The combination of a metal ion (M) and the oxide support (S) can lead to various types of supported metal oxide catalysts.

the dispersion of the metal oxides, but also directly affect the catalytic activity and/or selectivity of these supported metal oxides. Thus, heterogeneous catalysis over supported metal oxides is a typical example of "chemistry at interfaces." This interfacial chemistry plays a pivotal role at two distinct levels. First of all, there is the adsorption of reagent molecules from the gas or liquid phase at the catalyst surface, followed by bond breaking and formation, and finally desorption of the reaction products. There is, however, also a solid–solid interaction operative at the metal oxide–support interface. It is this metal oxide–support interaction that directly affects the coordination environment of the metal oxide, etc. and thus indirectly its ability to activate the adsorbed molecules, i.e., to influence the catalyst performances.

It is important to stress here that metal oxides can be dispersed on supports because the deposition process results in a lowering of the surface free energy relative to the high free energy of the exposed oxide supports. It is this lowering of energy that results in the formation of specific molecular structures of metal oxides, which would otherwise not be observed in the absence of the oxide support. This driving force is so strong that the specific molecular structures of the metal oxides are spontaneously formed when a physical mixture of a crystalline metal oxide and an oxide support are heated in air. Thus, energy minimizations are a crucial aspect in formation of supported metal oxide catalysts.

The goal of this chapter is to discuss the chemical phen ena taking place at the supported metal oxide–gas/liquid metal oxide–support interfaces for each stage of the life s of a heterogeneous catalyst, i.e., catalyst preparation, c lyst activation, catalytic action, and catalyst deactivation. S information is not only crucial for developing relevant (pre ably quantitative) structure/composition–activity/selecti relationships, but also for understanding the underlying p ciples of designing supported metal oxides for a particu catalytic application. Obtaining such important informati requires the intelligent combination of three approaches:

(1) spectroscopic characterization of the supported met oxides as a function of the support type/compositio and the metal oxide loading, preferably under *in sit* or catalytically relevant conditions;
(2) determination of the catalytic activity/selectivity of t supported metal oxides as a function of the support type/composition and the metal oxide loading; and
(3) theoretical calculations on model clusters, which closely resemble the supported metal oxides. This requires realistic cluster models and accurate comput simulation programs. It is, however, far from simple to have reliable cluster models, which accurately describe the supported metal oxides.

Each of these approaches will be illustrated in this chapte for one or more selected examples of supported metal oxid catalysts.

1.2. Scope of the Review

The main focus of this chapter is on the inorganic aspect of supported metal oxide catalysts. Thus, we will concentrate on the physicochemical structure of the supported metal oxides before, during, and after catalytic action and its relation with catalytic activity, selectivity, and stability. The review article starts with a brief introduction to the general properties of metal oxides, while the second section deals with the preparation of supported metal oxides, and the different preparation methods and supports currently available. The most important characteristics of the many supports used nowadays for preparing supported metal oxide catalysts are described.

Table I. Industrial Applications of Some Supported Metal Oxide Catalysts [10]

Active metal oxide	Support	Catalyzed reaction	Reaction conditions
V_2O_5	TiO_2	*o*-Xylene to phthalic anhydride	400–450°C, 1.2 bar
V_2O_5	TiO_2	Reduction of NO_x with NH_3	450°C, 1 bar
CrO_3	Al_2O_3	Dehydrogenation of alkanes	500–600°C, 1 bar
CrO_3	SiO_2	Polymerization of olefins	50–150°C, 20–30 bar
MoO_3	Al_2O_3	Demethylation of toluene	500–600°C, 20–40 bar
MoO_3	Al_2O_3	Hydrocracking of vacuum distillates	320–420°C, 100–200 bar
MoO_3	Al_2O_3	Metathesis of olefins	100–125°C, 10 bar
WoO_3	SiO_2	Metathesis of olefins	350–425°C
Re_2O_7	Al_2O_3	Metathesis of olefins	20–100°C, 60 bar

Table II. Common Metal Oxides of First, Second and Third Row Transition Metals, Together with Their Electron Configurations [18]

Row	Transition metal (electron configuration)	Oxidation state of the transition metal ion in metal oxides						
		+1	+2	+3	+4	+5	+6	+7
1	Sc ([Ar]$3d^1 4s^2$)			Sc_2O_3				
	Ti ([Ar]$3d^2 4s^2$)		TiO		TiO_2			
	V ([Ar]$3d^3 4s^2$)		VO	V_2O_3	VO_2	V_2O_5		
	Cr ([Ar]$3d^5 4s^1$)			Cr_2O_3	CrO_2		CrO_3	
	Mn ([Ar]$3d^5 4s^2$)		MnO	Mn_2O_3	MnO_2			(Mn_2O_7)
	Fe ([Ar]$3d^6 4s^2$)		FeO, (Fe_3O_4)	Fe_2O_3, (Fe_3O_4)				
	Co ([Ar]$3d^7 4s^2$)		CoO, (Co_3O_4)	(Co_3O_4)				
	Ni ([Ar]$3d^8 4s^2$)		NiO					
	Cu ([Ar]$3d^{10} 4s^1$)	Cu_2O	CuO					
	Zn ([Ar]$3d^{10} 4s^2$)		ZnO					
2	Y ([Kr]$4d^1 5s^2$)			Y_2O_3				
	Zr ([Kr]$4d^2 5s^2$)				ZrO_2			
	Nb ([Kr]$4d^3 5s^2$)		NbO		NbO_2	Nb_2O_5		
	Mo ([Kr]$4d^5 5s^1$)				MoO_2		MoO_3	
	Tc ([Kr]$4d^6 5s^1$)				TcO_2			Tc_2O_7
	Ru ([Kr]$4d^7 5s^1$)				RuO_2			RuO_4
	Rh ([Kr]$4d^8 5s^1$)			Rh_2O_3	RhO_2			
	Pd ([Kr]$4d^{10} 5s^0$)		PdO					
	Ag ([Kr]$4d^{10} 5s^1$)	Ag_2O						
	Cd ([Kr]$4d^{10} 5s^2$)		CdO					
3	La ([Xe]$4f^{14} 5d^1 6s^2$)			La_2O_3				
	Hf ([Xe]$4f^{14} 5d^2 6s^2$)				HfO_2			
	Ta ([Xe]$4f^{14} 5d^3 6s^2$)		(TaO)		TaO_2	Ta_2O_5		
	W ([Xe]$4f^{14} 5d^4 6s^2$)				WO_2		WO_3	
	Re ([Xe]$4f^{14} 5d^5 6s^2$)				ReO_2	Re_2O_5	ReO_3	Re_2O_7
	Os ([Xe]$4f^{14} 5d^6 6s^2$)				OsO_2			OsO_4
	Ir ([Xe]$4f^{14} 5d^7 6s^2$)				IrO_2			
	Pt ([Xe]$4f^{14} 5d^9 6s^1$)				PtO_2			
	Au ([Xe]$4f^{14} 5d^{10} 6s^1$)			(Au_2O_3)				
	Hg ([Xe]$4f^{14} 5d^{10} 6s^2$)		HgO					

Section 3 will cover the different techniques used to characterize these supported metal oxides. It will be shown that sufficient detailed information can only be obtained by an intelligent combination of complementary spectroscopic techniques. Their application definitely results in a better understanding of catalyst preparation, calcination, activation, reaction, and deactivation. In a final chapter, an overview of the many applications of supported metal oxides in the field of heterogeneous catalysis is given. In addition, four selected examples will be discussed in more detail to appreciate the complexity of these materials. The chapter closes with some concluding remarks and a look into the future.

2. PROPERTIES OF METAL OXIDES

It is generally known that metal ions can form one or more metal oxides, i.e., compounds with oxygen as a lattice anion [7, 18]. Table II gives an overview of the most common and rather stable oxides of first-, second-, and third-row transition metals. These metals are listed in Figure 4, and their electron configuration is included in Table II. It is clear that different metal oxides can be formed from the same transition metal ion, depending on its oxidation state and coordination requirements. In this respect, V, Cr, Mn, Nb, and Re have the richest metal oxide chemistry. The difference between oxides of V^{5+} and Cr^{6+} is, for example, that Cr^{6+} can only have a tetrahedral coordination, whereas V^{5+} ions can be present in metal oxides in both an octahedral and tetrahedral coordination.

Table II is a simplification because

1. The surface of metal oxides is not perfect and there are many defects, steps, etc. present in these materials.
2. Transition metals frequently show nonstoichiometric behavior in their oxide composition.

One can easily understand that these two aspects are even more pronounced when the metal oxides are dispersed on an inorganic support. Other metal oxides may contain the transition metal ion in two different oxidation states. Examples are Co_3O_4 and Fe_3O_4. There are also tetroxides in nature. Examples of tetroxides are OsO_4 and RuO_4.

	IIIa	IVa	Va	VIa	VIIa	VIII	Ib			IIb
3d	Sc	Ti	V	Cr	Mn	Fe	Co	Ni	Cu	Zn
4d	Y	Zr	Nb	Mo	Tc	Ru	Rh	*Pd*	*Ag*	Cd
5d	La	Hf	Ta	W	Re	Os	Ir	*Pt*	*Au*	Hg

Fig. 4. Periodic table, including the 3d, 4d, and 5d transition metals. The scope of the paper is limited to the elements indicated by the gray shading.

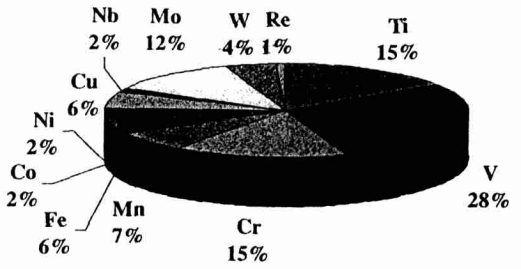

Fig. 5. Overview of the number of literature hits (expressed as a percentage) for different supported metal oxide catalysts. These results were obtained from the Web of Science of the Institute of Scientific Information.

A common way of classifying oxides is based on their acid–base properties. Metal oxides can then be classified as acidic (e.g., CrO_3 and V_2O_5), basic (e.g., La_2O_3), or amphoteric (e.g., ZnO). In this respect, it is important to know that acidity mostly increases with increasing oxidation state of the transition metal ion: e.g., $MnO < Mn_2O_3 < MnO_2 < Mn_2O_7$. A final comment about Table II can be made concerning the noble metals, Au, Pt, Pd, and Ag, which form stable oxides (Au_2O_3, PtO_2, PdO, and Ag_2O). In what follows, we will limit ourselves to the transition metals indicated by the gray shadings in Figure 4 because the corresponding transition metal oxides are frequently encountered in catalyst formulations and are well studied via many characterization techniques.

Figure 5 gives an overview of the number of literature hits obtained for each of these transition metal ions in the period 1990–1999 with the keywords "supported *x* oxide" or "supported *x* oxides," where *x* is titanium, vanadium, chromium, manganese, iron, cobalt, nickel, copper, zinc, niobium, molybdenum, tungsten, or rhenium. These results were obtained from the Web of Science of the Institute of Scientific Information. The most frequently studied supported metal oxide catalysts are those with vanadium, and about 30% of all publications in the field are devoted to this transition metal. Other very important transition metals are Cr, Ti, and, to a lesser extent, Mo. Not frequently studied transition metals in the field of supported metal oxide catalysis are Re, Nb, Ni, and Co. As a consequence, most of the examples, which will be discussed in this chapter, are supported vanadium oxides and chromium oxides, although the developed concepts are equally valid for the other supported transition metal oxides as well.

3. PREPARATION OF SUPPORTED METAL OXIDES

3.1. Supports and Their Properties

Supports used for the preparation of metal oxide catalysts are usually inorganic oxides with micropores, mesopores, and/or macropores and a high surface area [12]. They can be either amorphous or crystalline, and in the latter case the channel system can be one-, two-, or three-dimensional. A whole variety of supports are commercially available for preparing supported metal oxide catalysts. Table III gives an overview of some of the most important supports used nowadays catalyst suppliers, together with supports, which are mor academic interest but certainly will have applications in future. Frequently used supports are silica, alumina, tita clays, and zeolites. Some properties of these supports are included in this table.

The selection of a support for a specific catalytic appli tion is based on its properties, which can be summarized follows [12]:

1. Intrinsic physicochemical properties of the support. T support material has a direct influence on the dispersion metal oxides on the surface. This is possible because of t presence of, e.g., hydroxyl groups. These hydroxyl grou are able to anchor metal oxides via typical S-O-M chem cal bonds (where S is the support and M is the metal oxi compound). The total number and the intrinsic properties these hydroxyl groups have a direct influence on the disper ing power of a specific support. For example, silica suppor have a relatively low number of hydroxyl groups, and thes hydroxyl groups are more acid-like. Both properties resu in a weak dispersion of the metal oxide, and, consequentl metal oxide clusters on the silica surface are formed instea of well-dispersed metal oxides. An example is the formatio of Cr_2O_3 clusters on a silica surface on a CrO_3/SiO_2 cata lyst [19]. The support material can also stabilize specific oxi dation states and molecular structures of the metal oxides on its surface. This ability originates from the intrinsic chemistry (e.g., hardness/softness) of the support, which is related to the chemical composition. For example, silica supports will preferably stabilize Cr^{2+} after CO reduction, whereas Cr^{3+} ions are stabilized on an alumina support after an identical pretreatment [19].

2. Chemical inertness/reactiveness of the support. Inorganic oxides, such as alumina, however, cannot be regarded as inert because they possess reactive groups at their surface. These reactive groups can have acid, basic, or redox properties and are, as discussed above, the responsible sites for anchoring the metal oxides to the support. They can, however, also catalyze undesirable side reactions. A typical example is the Houdry CrO_3/Al_2O_3 catalyst for the dehydrogenation of light alkanes, such as isobutane and propane, in the absence of oxygen. The addition of small amounts of K^+ to the alumina support of this catalyst is necessary to kill the acidic hydroxyl groups responsible for cracking and coke formation [17]. Sometimes these reactive groups at the surface can also be beneficial in a catalytic process and may result in the formation of bifunctional catalysts. An example is the activation of methane over Fe/H-ZSM-5 catalysts in the absence of oxygen at high temperatures [20]. Methane is converted to ethylene over dispersed Fe_2O_3/Fe_3O_4 clusters dispersed predominantly at the outer surface of the zeolite. The ethylene formed is then further converted to aromatic compounds over the Brönsted acid sites located at the internal surface of the zeolite.

3. Desirable mechanical properties and stability during preparation and under reaction and regeneration conditions of

Table III. Overview of the Inorganic Supports Used for Preparing Supported Metal Oxide Catalysts

Type	Structure	Pore dimensions	Support
Amorphous			SiO_2
			Al_2O_3
			$SiO_2.Al_2O_3$
			TiO_2
			ZrO_2
			MgO
			La_2O_3
			SnO_2
			HfO_2
			ZnO
Crystalline	Two-dimensional		Clay minerals
			Layered double hydroxides
	Three-dimensional	Microporous	Aluminosilicates
			Silicates
			Aluminophosphates
			Metallophosphates
		Mesoporous	Mesoporous crystalline materials
			Hexagonal mesoporous silica
			Aluminophosphates

the support. First of all, the support has to keep its mechanical properties during catalyst preparation. Indeed, the support has to resist acidic or basic ion exchange of impregnation solutions. Second, the catalyst support has to possess sufficient attrition resistance, hardness, and compressive strength in the catalytic reactor. Otherwise, fines can be produced during catalytic operation, which may result in a pressure drop in the catalytic bed. In the case where the catalyst is used in liquid phase catalysis, resistance to erosion by the fluids is also necessary. A catalyst support with good stability will change only slowly during the catalyst lifetime. However, in some applications the support has to be strong enough to withstand the catalytic reactor conditions, but be able to break up because of the catalytic reaction going on in the pores of the catalyst support. Here, the catalyst support is gradually dispersed in the material, which is produced by the catalyst. An illustrative example is the polymerization of ethylene over CrO_3/SiO_2 catalysts [21, 22]. These catalysts must fragment during ethylene polymerization, otherwise the pores of the silica support remain blocked by the polymers initially formed within the pore structure. In this case, no appreciable and longstanding polymerization activity is observed, and thus silica supports with special properties have to be prepared for making highly active ethylene polymerization catalysts. Finally, the catalyst support has to possess sufficient chemical stability against, e.g., steaming conditions. An example is the stability of ultrastable Y (USY) catalysts used in the FCC (fluid catalytic cracking) process during relatively severe catalyst regeneration conditions. These conditions do not allow the use of the classic zeolite Y material in these applications because the presence of steam in the regeneration step results in dealumination of the zeolite material. This also points to another important characteristic of the catalyst support, namely its regenerability. Indeed, it is only in theory that the catalyst is found intact at the end of the reaction and all catalyst ages. They must be regenerated, which is most often done by an oxidative treatment. This implies that the catalyst support has to preserve its properties during successive regeneration treatments in a catalytic reactor. This is far from obvious.

4. Surface area and porosity of the support, including the pore size and pore size distribution. A high surface area is usually, but not always, desirable because the active metal oxide is then well dispersed over the support surface. High surface areas often imply small pores, which could become plugged during impregnation. This can be a problem when high metal oxide loadings are needed. Pore sizes of the support material are also crucial when large preformed metal complexes are ion exchanged onto the support [23]. The dimensions of the pores, in particular the dimensions of the ring of oxygen atoms of a molecular sieve, will then determine which metal complexes can be immobilized on the specific support surface. These pores can also block reagent molecules during a catalytic reaction to enter the pore system of a heterogeneous catalyst. This is responsible for the shape selectivity of such catalysts.

5. Morphology of the support. The morphology refers to the form and grain size of the catalyst support particle. It is mainly determined by the process characteristics. For moving and boiling bed catalytic reactors the spherical form is recommended, to reduce the problems of attrition and abrasion. Fluid bed catalytic reactors need spherical powder, whereas in a fixed catalytic bed, beads, rings, pellets, extrudates, or flakes can be used. Their form and dimensions have a strong influence on the pressure drop through the catalytic bed. This pressure drop must be high enough to ensure an even distribution of the reaction fluid across the catalytic bed, but it must not be so high as to cause an increase in the cost of compressing gases.

6. Cost and reproducibility of the properties of the support. Even when a support possesses all of the ideal properties, which are described above, its cost has to be as low as possible. In this respect, zirconia supports are much less used in industrial catalysis in comparison with silica and alumina supports. Reproducibility of the support refers to its constant quality, which allows making identical catalyst formulations for an extended time period.

3.2. Preparation Methods

The preparation of supported metal oxide catalysts is a very important step because it significantly affects the three most important characteristics of the final catalyst product, i.e., its catalytic activity, catalyst selectivity, and catalyst lifetime [2]. Therefore, scientists and catalyst producers should "design" their catalyst for a specific application [24]. Despite the large number of publications and patents about catalyst preparation, the field of "catalyst design" can be still considered to be in its infancy. It involves the precise control over the nature (oxidation state, coordination environment, dispersion, etc.) of the supported active site at the molecular level in a reproducible manner. This is far from easy, and future research has to be directed toward a better understanding of the basic aspects of catalyst preparation through the use of *in situ* spectroscopic measurements. This would allow researchers to identify the most crucial steps in the preparation method and to define the most appropriate *modus operandi* for preparing an industrial catalyst. In this respect, it is important to recall the definition of catalyst preparation by Richardson [25]: "Catalyst preparation is the secret to achieving the desired activity, selectivity and life time." Catalyst preparation is thus defined as a strategic domain in chemical industries, which is often not disclosed in the open literature. It is also a field with great potential because important improvements in catalyst performance can be obtained by simply fine-tuning the different preparation steps of a specific catalyst.

There are two main stages in the preparation of supported metal oxide catalysts. In a first stage, the active metal component precursor is deposited on the oxidic support. The second stage consists of a transformation of the deposited metal precursor into a metal oxide dispersed at the support surface. This transformation process can be achieved by a heat treatment of the precursor material in oxygen or air, often referred to as the calcination step (formation of supported metal oxides). Other transformation processes are sulfidation (formation of supported metal sulfides), carburization (formation of supported metal carbides), and metallization (formation of supported metals) (Fig. 1). Because this chapter is limited to metal oxides supported on inorganic surfaces, the latter transformation processes will not be discussed, but details about such catalytic systems can be found in the literature [1].

A vast majority of deposition methods involve aqueous or nonaqueous solutions of the metal component precursor. The interaction between the metal precursor and the support then takes place at the liquid–solid interface. In some cases, deposition can also be performed with a metal precursor in the gasphase and then involves chemical phenomena at the gas–solid interface. There are several deposition methods for the preparation of supported metal oxide catalysts in the literature. In what follows, we will briefly describe the main preparation methods currently used. Their advantages and disadvantages will also be discussed. For a detailed discussion, we refer to several excellent textbooks and review papers [1, 3, 10, 12, 15].

The most simple and widely used deposition method for making supported metal oxide catalysts is impregnation with aqueous and nonaqueous solutions of metal oxides. The term "impregnation" refers to a procedure whereby a certain volume of an aqueous or nonaqueous solution containing the specific metal component precursor is totally adsorbed into the pores of an inorganic oxide. One of the drawbacks here is that, e.g., V_2O_5 and Cr_2O_3 have a (very) low solubility in aqueous and nonaqueous solutions. Therefore, the use of, e.g., NH_4VO_3 or CrO_3 in water and NH_4VO_3 dissolved in oxalic acid is recommended [26]. In the latter case, the resulting deep blue solution contains the compound $(NH_4)_2(VO(C_2O_4)_2)$, the vanadium being present as V^{4+}. Many other metal precursor salts are commercially available that are soluble in aqueous and nonaqueous solutions.

Ion exchange is another relatively simple method for the deposition of a metal precursor on an inorganic oxide. Ion exchange consists of replacing an ion in an electrostatic interaction with the surface of an inorganic support by another ionic species. This method requires an oxidic support with ion exchange capacity (IEC); i.e., the support material possesses a framework with an excess of negative or positive charges. An important example is a zeolite, in which, e.g., Na^+ cations are neutralizing the negative charges of the zeolite framework. These cations are not linked to the framework and can be (partially) exchanged for a metal ion species, such as Cu^{2+} and Co^{2+}. Metal complexes with a positive charge can also be exchanged onto these oxides. Zeolites, such as Na-ZSM-5, Na-mordenite, and Na-Y, are typical examples of crystalline oxides with cation exchange capacity (CEC). Other examples of crystalline materials with CEC properties are cationic clay minerals, such as hectorite, saponite, and laponite. Some inorganic oxides, however, possess anion exchange capacity (AEC) because of their positive framework charge. They can be used in the ion exchange of metal oxoanions, such as MoO_4^{2-} and CrO_4^{2-} [27]. An example is a hydrotalcite material, which is a layered double hydroxide (often referred to as LDH). This oxide can be considered an anionic clay material.

Another frequently used method is grafting, which is defined as the removal from solution of a metal precursor compound through interaction with the hydroxyl groups of the support. An example is the use of a solution of $VOCl_3$ in CCl_4 or $VO(acac)_2$ (with acac, acetylacetonate) in toluene to obtain a dispersed VO_x phase on inorganic oxides. In the case of the $VOCl_3$ salt there is a chemical reaction, taking place between the metal precursor and the hydroxyl groups of the support with the release of HCl. The interaction of

$VO(acac)_2$ or $Cr(acac)_3$ complexes with the support, depending on the support type and composition, is via either hydrogen bonding with the hydroxyl groups of the support or a real ligand exchange reaction with the release of Hacac (protonated acetylacetonate). This method is often referred to by the term "molecularly designed dispersion" or the MDD method because it allows control over the dispersion of the metal precursor at the support surface [28]. Multiple grafting is also possible and may result in the formation of a monolayer of MO_x covering the surface of the inorganic support.

The same processes of adsorption and/or chemical reaction may occur in the gas phase, and this method is then generally called chemical vapor deposition (CVD). CVD is a process in which an active component from a volatile inorganic or organometallic compound is laid down on the exterior surface of a support by reaction with its hydroxyl groups. Interesting metal precursor compounds for this deposition method are chlorides (e.g., VCl_4, CrO_2Cl_2, and $MOCl_5$), alkoxides (e.g., $Ti(OC_2H_5)_4$), and β-diketonates (e.g., $Cu(acac)_2$, $Cr(acac)_3$, and $VO(acac)_2$). The equipment used for catalyst preparation via the CVD technique is relatively simple and can be used in either a open or closed reactor system. A special mode of CVD is the ALE or atomic layer epitaxy technique [29, 30]. This technique allows better control of the build-up of supported metal species by the sequential introduction of the metal precursor compounds at an appropriate reaction temperature. The latter avoids the uncontrolled deposition through condensation of the reactants or their decomposition products. In this respect, chemisorption of the metal precursor is essential to obtaining well-defined metal oxide surface structures on the support surface.

Metal oxides and the inorganic supports—or their metal precursors—may also be coprecipitated from a solution containing precursor compounds of each element. This coprecipitation method usually produces an intimate mixing of the catalytic active phase and the support, but the active component is dispersed throughout the bulk as well as being on the surface. An example of such a procedure is the preparation of V_2O_5/TiO_2 catalysts starting from a mixed V^{4+} and Ti^{4+} solution, by the addition of NH_4OH. A related preparation method is isomorphous substitution, which is defined as the replacement of an element in the crystalline framework of molecular sieves by another element with similar cation radius and coordination requirements [31]. For example, both the Co^{2+} and Al^{3+} ions can be present under tetrahedral coordination and possess a similar cation radius. As a consequence, Co^{2+} can substitute for Al^{3+} in the framework of a microporous crystalline aluminophosphate, such as $AlPO_4$-5, resulting in the formation of a CoAPO-5 material. This molecular sieve can be prepared starting from a gel containing a small amount of a Co^{2+} salt (e.g., $CoCl_2$), an aluminium source (e.g., pseudoboehmite), a phosphorus source (e.g., H_3PO_4), a template molecule (e.g., triethylamine), and water. This synthesis mixture is then transferred after mixing in an autoclave, and the synthesis is conducted at high temperarures and pressures for several hours. After synthesis, a crystalline CoAPO-5 powder can be recovered from the synthesis mixture. In an analogous way, $Fe^{2+/3+}$, Cr^{3+}, V^{4+}, Ti^{4+}, Mn^{2+}, etc. can be incorporated into the framework of microporous and mesoporous crystalline aluminophosphates, silicates, and aluminosilicates.

A last example of a preparation technique is thermal spreading [32–34]. Here, a physical mixture of the metal oxide and the support is heated, and the metal oxide compound will start to spread over the supporting oxide. This results in a covering of the support by a thin layer of metal oxides and is thermodynamically driven because of a net lowering of the energy of the catalyst system. This method has been successfully used with, e.g., V_2O_5 or MoO_3 as metal oxide and Al_2O_3 as support for preparing V_2O_5/Al_2O_3 and MoO_3/Al_2O_3 catalysts.

Finally, an important comment has to be made about the specific preparation conditions, such as calcination temperature and time and the pH of the impregnation solution. Several important changes in the supported metal oxide catalysts may occur if these experimental conditions for preparing the catalysts are not properly adjusted or chosen. A first example is the dissolution or partial destruction of the oxidic support in an acid or basic solution used for, e.g., ion exchange and impregnation. Another is the formation of stable surface compounds of the metal precursor species with the support oxide when a very acidic impregnation solution is used. The latter can also occur when very high calcination temperatures are applied. The overall results are a lowering of the amount of the required active phase on the support surface and a change in the properties of the support material. Therefore, not only the specific preparation method, but also the preparation conditions have to be chosen carefully to obtain highly active and selective supported metal oxide catalysts.

3.3. Promoters

A heterogeneous catalyst consists of an active component and one or more promoters [10]. These substances are not themselves catalytically active but substantially increase the catalytic performances of a catalyst material. Promoters are the subject of great interest in catalyst research because of their remarkable influence on the activity, selectivity, and stability of a heterogeneous catalyst. The discovery of a specific substance acting as a promoter in a catalytic reaction is not based on systematic scientific research, but often on serendipity. The function of promoters, which are added to heterogeneous catalysts in amounts of a few percent, is not always clear, but their effect can be subdivided into four groups:

1. Structure promoters. These substances increase the selectivity of a heterogeneous catalyst by reducing the number of possible reactions for the adsorbed molecules at the catalyst surface and favoring the required reaction pathway.
2. Textural promoters. These promoters inhibit the agglomeration of catalyst particles to larger, less active structures during the reaction. Thus, they prevent the loss of active surface by sintering and increase the thermal stability of a heterogeneous catalyst.

Table IV. Examples of Some Promoters and Their Effect in Supported Metal Oxide Catalysis [10]

Promoters	Function
SiO_2	Increase thermal stability
ZrO_2	Increase thermal stability
K_2O	Poisons coke formation
HCl	Increases acidity
MgO	Slows sintering of active phase
Al_2O_3	Structure promotor
P	Increased metal oxide dispersion
B	Increased metal oxide dispersion

3. Electronic promoters. These substances are dispersed in the active phase and influence its electronic character and therefore the chemical binding of the reactant molecule.
4. Anti-poison promoters. These promoters protect the active site of a heterogeneous catalyst against poisoning by impurities (e.g., in feed).

Table IV gives an overview of some promoters used in heterogeneous catalysis. It is clear that the function of a promoter cannot be precisely defined, and often the four effects overlap for a typical catalyst promoter.

Promoters are often used to suppress the undesired activity of oxide supports, such as coke formation on an Al_2O_3 support. Coking is due to cracking reactions on acid centers, followed by an acid-catalyzed polymerization to give $(CH_x)_n$ chains, which cover the active sites of a heterogeneous catalyst and block the pores. Removal of this coke by incineration can lead to a loss of activity due to sintering. The addition of potassium is the most effective way to minimize the coking tendency of Al_2O_3 support; it is present, for example, in the industrial Houdry CrO_3/Al_2O_3 catalyst used for the catalytic dehydrogenation of alkanes in the absence of oxygen [17]. Another frequently added alkali metal is Na, which is known to be a promoter in WO_3/SiO_2 catalysts for alkene metathesis [10, 35]. The sodium ions prevent double-bond shift reactions during this industrial process.

Another example is the addition of structural promoters to increase the stability of oxide supports. Oxide supports can exist in numerous different phases, and for Al_2O_3 the preferred phase is γ-Al_2O_3. This oxide has a defect spinel structure with a high surface area and a certain degree of acidity. It can also form solid solutions with transition metal oxides, such as NiO, CoO, and Cr_2O_3. The γ-Al_2O_3 phase is gradually transformed into α-Al_2O_3 above 900°C. The α-Al_2O_3 phase has a hexagonal structure and a smaller surface area. Such high temperatures can occur during catalyst regeneration, although a slow phase transition can also take place at lower temperatures. This shortens the catalyst lifetime, and the addition of small amounts of SiO_2 and ZrO_2 to γ-Al_2O_3 shifts the transition to higher temperature and consequently increases the stability and lifetime of a heterogeneous catalyst. A last example of a promoter effect is the addition of K_2SO_4 to supported vanadium oxide catalysts used for the selective oxidation of methanol to formaldehyde. This addition has a positive effect on the reaction rate and increases the selectivity to formaldehyde. Here, the potassium is assumed to release electrons to the metal oxide, which results in an increase in the rate of the oxidation reaction.

4. CHARACTERIZATION OF SUPPORTED METAL OXIDES

The characterization of the molecular structures of metal oxides on the surface of an inorganic oxide is rather involved, since deposition of the metal oxide on the support material can result in (1) isolated metal ions; (2) a two-dimensional overlayer of metal oxides, and/or (3) three-dimensional metal oxide crystallites [2]. This is schematically illustrated in Figure 6 for supported vanadium oxide catalysts. The vanadium oxide species can be present as monomeric species, polymeric species, amorphous metal oxides, and crystalline metal oxides (V_2O_5) on the surface of an amorphous support.

Moreover, each of these phases can simultaneously possess several different molecular structures of the metal oxide, and the exact structure of each surface species is strongly dependent on the (catalytic) conditions. This reinforces the idea that supported metal oxide catalysts are very complex materials. Spectroscopic, microscopic, diffraction, and reaction techniques are necessary to provide detailed information about the molecular structures of the supported metal oxide. These characterization techniques must be capable of discriminating between these different states and of quantifying the individual oxidation states of the metal ions. It is clear that the use of a battery of different characterization techniques is recommended, and this strategy is often referred to as the multitechnique approach.

Characterization techniques for investigating supported metal oxide catalysts can be subdivided into five groups [2, 8, 9]:

- Physical characterization techniques: pore volume, pore distribution, and surface area determinations. This is possible, for example, via liquid N_2 adsorption-desorption measurements.
- Temperature-programmed techniques: temperature-programmed reduction (TPR), temperature-programmed oxidation (TPO), temperature-programmed desorption (TPD), and temperature-programmed reaction spectroscopy (TPRS)
- Spectroscopic techniques: infrared spectroscopy (IR), Raman spectroscopy (RS), electron spin resonance (ESR), X-ray photoelectron spectroscopy (XPS), diffuse reflectance spectroscopy in the UV-Vis-NIR region (DRS), nuclear magnetic resonance (NMR), X-ray absorption spectroscopy (XAS, also known as EXAFS-XANES), Mössbauer absorption spectroscopy and Mössbauer emission spectroscopy (MES), ultraviolet X-ray photoelectron spectroscopy (UPS), low-energy ion scattering (LEIS), Rutherford backscattering (RBS), thermal desorption

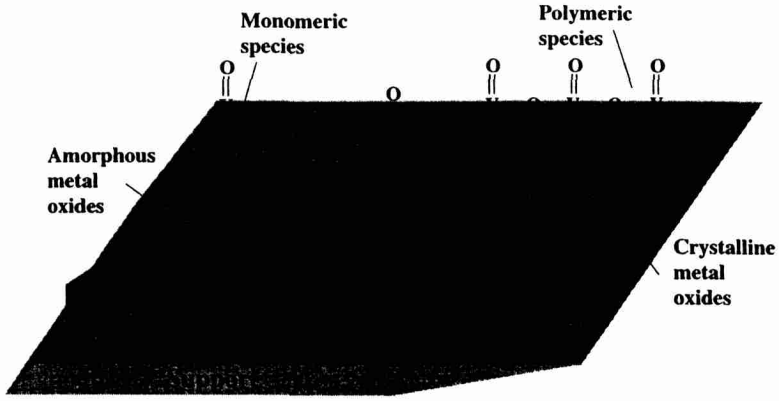

Fig. 6. Schematic representation of the complexity of the physicochemical structure of supported vanadium oxide catalysts. The supported metal oxides can be present as a monomeric species, polymeric species, crystalline metal oxides, and amorphous metal oxides. This complexity makes a complete characterization of these systems an involved process.

spectroscopy (TDS), secondary ion mass spectroscopy (SIMS), secondary neutral mass spectroscopy (SNMS), electron energy loss spectroscopy (EELS), and Auger electron spectroscopy (AES)

- Diffraction techniques: X-ray diffraction (XRD) and low-energy electron diffraction (LEED)
- Microscopic techniques: scanning electron microscopy (SEM), atomic force microscopy (AFM), field emission microscopy (FEM), field ion microscopy (FIM), scanning tunneling microscopy (STM), and transmission electron microscopy (TEM).

These techniques can provide detailed information about the physical properties and bulk chemical and surface chemical composition of the catalyst, the oxidation states and the coordination environment of the metal ion present in the catalyst material, the concentration and dispersion of the metal ion, and the morphology of the catalyst material. Details about all of these characterization techniques and their application to the field of heterogeneous catalysis can be found in several textbooks and book chapters [1, 4–6, 8, 9, 15]. In any case, spectroscopic techniques are the preferred characterization techniques for the elucidation of the physicochemical structure of supported metal oxide catalysts because the spectroscopic data are fingerprints of the local structure of the catalyst material, which cannot be obtained with other techniques.

All of the mentioned spectroscopic techniques for studying supported metal oxides can be derived from the scheme given in Figure 7. This pictorial representation is generally known as the Propst diagram, and the circle in the center represents the supported metal oxide to be analyzed [6]. Ingoing arrows indicate the various methods used to excite the catalyst sample, and the possible responses of the heterogeneous catalyst to that excitation are indicated by the outgoing arrows. For example, one can irradiate with photons and measure the energy distribution of electrons that are emitted from the catalyst surface because of the photoelectric effect. This forms

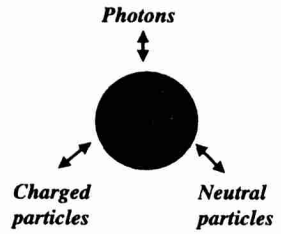

Fig. 7. Propst diagram summarizing the different spectroscopic techniques used for studying supported metal oxide catalysts. The circle is the supported metal oxide catalyst, the inward arrow stands for an excitation of the transition metal oxide, and the outward arrow indicates how the information can be extracted.

the basis of XPS. A single combination of inward and outward arrows may lead to distinct spectroscopies, depending on what property of the sample is measured. This is the case for IR and RS. The most frequently used spectroscopic techniques for the study of metal oxide catalysts are ESR, IR, RS, XPS, DRS, and XAS [2]. Their advantage is that they can be used to characterize real catalytic systems and that they are not limited to model systems.

None of the mentioned characterization techniques will be capable of providing all of the information needed for a complete characterization of supported metal oxide catalysts. The successful characterization of these materials requires—as was mentioned—a multitechnique approach. This approach implies an intelligent combination of different complementary techniques. In this respect, it is important to stress that

1. Each characterization technique has its own sensitivity toward specific oxidation states and molecular structures of supported metal oxides. This implies that catalyst scientists have to be very careful if their reasonings and models about active sites and reaction intermediates are based solely on one characterization technique. For example, RS seems to be very powerful in discriminating between monomeric and polymeric metal oxides in their highest valence state. Lower valence states, however, are very difficult to observe by RS, and often

fluorescence will overshadow the weak Raman scattering of the supported metal ions of interest. Another example is ESR, which is only sensitive to metal oxides, which have paramagnetic properties. This can be also an advantage because it can make the spectroscopic data easier to interpret.

2. Characterization techniques can be sensitive to either the bulk or the surface of a supported metal oxide. A surface technique becomes surface sensitive if the particles to be detected (e.g., electrons) come from the outer layers of the catalytic material only. This is the case for XPS and is related to the small mean free path of electrons. The consequence is that such measurements have to be conducted in a vacuum, which conflicts with the wish of catalyst scientists to study heterogeneous catalysts under realistic reaction conditions. On the other hand, many techniques are bulk techniques and give information about the whole catalyst sample. Examples are IR, DRS, XAS, ESR, and RS. The last technique, however, often suffers from fluorescence, which prevents well-resolved spectroscopic data from being obtained.

3. Most spectroscopic studies have been conducted up to now under conditions that were often far from real catalytic conditions [14]. Such studies are not sufficient to understand the molecular phenomena going on at the catalyst surface, and therefore researchers are currently developing spectroscopic tools that allow them to study supported metal oxides while they are in reaction. This is the field of *in situ* spectroscopy and requires the use of specially designed reaction/spectroscopic cells. This methodology is schematically illustrated in Figure 8. Conducting real in situ spectroscopic measurements is far from simple because the optimal conditions for performing spectroscopic and catalytic measurements are mostly not identical, and there will be always a c promise between the two types of measurements. The co quences of this compromise are a lower catalytic activity less resolved spectroscopic data. It is possible to conduc *situ* measurements of supported metal oxides with DRS, X ESR, IR, and RS.

Figure 9 gives an overview of the whole lifespan o supported metal oxide catalyst from its genesis to catal deactivation and regeneration. In a first step, the metal ox catalyst is prepared, for example, by an impregnation s with an aqueous solution containing the metal ion (M) on t support material (S). The obtained hydrated material is th dried and calcined in an oxygen-rich environment. This ma rial (MO_x^{n+}-S) is a precursor material because it is not y active in a catalytic application and it should be first ac vated. Activation is often a reduction step in which the me oxide is reduced to a lower oxidation state in the presence

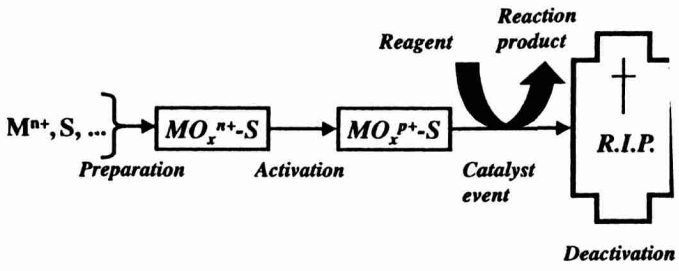

Fig. 9. The life span of a supported metal oxide catalyst, indicating the preparation, activation, catalytic event, and deactivation process of the catalyst material. M and S are the metal ion and support, respectively.

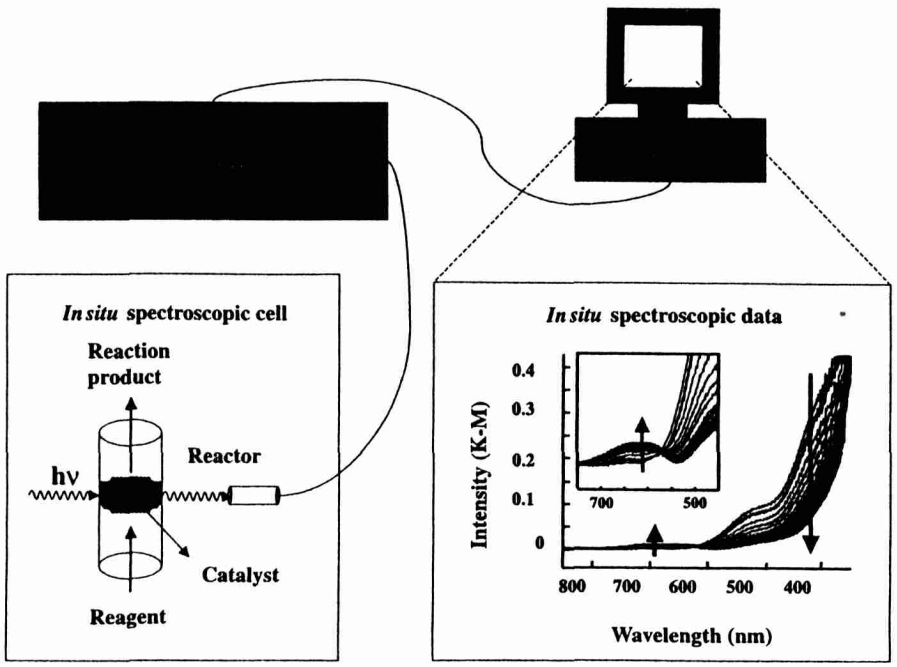

Fig. 8. Schematic representation of an *in situ* spectroscopic characterization study of supported metal oxide catalysts. The catalytic reaction is taking place in a specially designed *in situ* spectroscopic cell, which makes it possible to obtain relevant spectroscopic data of the working catalyst. The data are obtained for a CrO_3/SiO_2 alkane dehydrogenation catalyst.

CO or H_2 at relatively high temperatures. The obtained inorganic material (MO_x^{p+}-S with $p < n$) is catalytically active and will be able to convert a specific reactant molecule, to the desired reaction product molecule and this with a high activity and selectivity. Gradually, the catalyst material will deactivate because of coke formation or a change in the dispersion of the supported metal oxides.

We will now apply different (*in situ*) spectroscopic techniques to understand the different stages in the lifespan of supported metal oxide catalysts from a fundamental point of view. The developed concepts are also valid for other supported metal oxide catalysts.

4.1. Catalyst Preparation

In what follows, we will discuss the preparation of supported metal oxide catalysts made via an impregnation of a metal oxide-containing solution on a series of amorphous oxide supports. As an example, we start with the preparation of supported vanadium oxide catalysts, and later on a detailed comparison will be made with other supported metal oxides. It is important to stress here that the same molecular structures will be observed on the supports when the catalyst is rehydrated after a calcination step, and thus there is a dynamic interaction between the molecular structures of the metal oxides under hydrated or ambient conditions and dehydrated conditions. In other words, hydration and dehydration of supported metal oxide catalyts are reversible processes. The ambient conditions correspond here to room temperature and ambient air.

Supported vanadium oxide catalysts are industrially important because of their excellent catalytic performances in selective oxidation reactions and in the selective catalytic reduction of NO_x with NH_3 [36, 37]. Examples are the catalysts V_2O_5/TiO_2, V_2O_5/Al_2O_3, V_2O_5/SiO_2, and V_2O_5/ZrO_2. The specific molecular structure of the deposited V_2O_5 can be measured with RS, solid-state ^{51}V NMR, XANES-EXAFS, and DRS. All of these spectroscopic techniques have unambiguously shown that the molecular structure of solvated surface V^{5+} species present on these amorphous supports is dependent on the net pH at which the oxide surface possesses a zero surface charge. This pH value is also called the point of zero charge (PZC) or isoelectric point (IEP) of the support. It is mainly determined by the composition of the support and, as a consequence, SiO_2, Al_2O_3, ZrO_2, TiO_2, and MgO have different IEP values (Table V). MgO has a high IEP value of 11, indicating a basic support surface, whereas a SiO_2 support has more acid-like properties. Al_2O_3 supports are known to have amphoteric properties. This difference originates from the thin film containing water molecules, which are present on the support surface. The hydroxyl population of the support is therefore subject to pH-dependent equilibrium reactions. These equilibrium reactions can be written as follows:

$$X\text{-}OH_2^+ \leftrightarrow X\text{-}OH + H_s^+ \quad (1)$$

$$X\text{-}OH \leftrightarrow X\text{-}O^- + H_s^+ \quad (2)$$

$$H_s^+ \leftrightarrow H^+ \quad (3)$$

with X = Si, Al, Zr, Ti, or Mg; H_s^+ and H^+ represent the surface and solution protons, respectively. The lower the IEP of the amorphous oxide, the more the equilibria of the reactions (1)–(3) are driven to the right. The higher the H^+ concentration near the surface of the support, the more the equilibria of vanadium oxide species in the aqueous film near the support surface are driven toward the formation of decavanadate ($V_{10}O_{28}$) species. Indeed, spectroscopies have shown that in aqueous solutions starting from the alkaline side, orthovanadate (VO_4), pyrovanadate (V_2O_7), metavanadate ($(VO_3)_n$), and decavanadate ($V_{10}O_{28}$) are progressively formed. Hence, the structure of the vanadium oxide species follows the aqueous chemistry of V^{5+} as a function of the pH, and the main spectroscopic results for the catalysts V_2O_5/MgO, V_2O_5/Al_2O_3, V_2O_5/SiO_2, V_2O_5/TiO_2, V_2O_5/ZrO_2 with low V_2O_5 loading are summarized in Table V. These observations confirm the mentioned reasoning about the molecular structure of supported metal oxide catalysts under ambient conditions. It allows prediction of the molecular structures of supported metal oxide catalysts under ambient conditions [38].

When the vanadium oxide loadings on the amorphous supports increase two effects come into play:

1. The pH near the surface is lowered because of the presence of the acidic-like V_2O_5 oxides, and this pH value decreases with increasing V_2O_5 loading.
2. The dispersion depends on the available surface area as well as the availability of surface hydroxyl groups.

The two factors influence the surface chemistry of V^{5+} species in the same direction, i.e., toward the formation of decavanadate ($V_{10}O_{28}$) species (Table V). Thus, decavanadate ($V_{10}O_{28}$) species are even formed on an Al_2O_3 support at relatively high V_2O_5 loading. Factor 2 also implicates that high-surface-area supports, such as alumina, will give rise to relatively less decavandate species ($V_{10}O_{28}$) at high V_2O_5 loadings because more surface area is available to disperse metavanadate ($(VO_3)_n$) species.

The above finding that the surface vanadium oxide species present on hydrated oxide under hydrated conditions can be correlated with the IEP of the support suggests that this approach should also hold for other surface metal oxide systems (CrO_3, MoO_3, WO_3, and Re_2O_7) [38]. This is indeed the case, and Table V lists the observed surface metal oxide species found for chromium oxide, molybdenum oxide, tungsten oxide, and rhenium oxide on several oxide supports. Only monomeric ReO_4 is present in aqueous solutions, and consequently only ReO_4 species are present on all of the hydrated oxide supports examined. Chromium oxide is present as CrO_4 in basic solutions and as Cr_2O_7 in acidic solutions. At very low pH values, Cr_3O_{10} and Cr_4O_{13} species exist in aqueous solutions. The observed surface chromium oxide species present on the hydrated oxide supports follow the trend predicted from the IEP values of the supports. In the case of molybdenum and tungsten oxide, MoO_4 and WO_4 are present in basic solutions, whereas polyoxoanions are the major species ion acidic

Table V. Surface Metal Oxide Species on Different Hydrated Amorphous Oxide Supports [33]

Metal oxide	Oxide	IEP	Molecular structure of the metal oxide at low metal oxide loading	Molecular structure of the metal oxide at high metal oxide loading
V_2O_5	MgO	11	VO_4,[a] V_2O_7, $(VO_3)_n$	VO_4,[a] V_2O_7,[a] $(VO_3)_n$
	Al_2O_3	8	$(VO_3)_n$[a]	$(VO_3)_n$, $V_{10}O_{28}$[a]
	TiO_2	6	$(VO_3)_n$,[a] $V_{10}O_{28}$[a]	$V_{10}O_{28}$[a]
	ZrO_2	6	V_2O_7, $(VO_3)_n$,[a] $V_{10}O_{28}$[a]	$V_{10}O_{28}$[a]
	SiO_2	2–4	O_h[b]	V_2O_5
CrO_3	MgO	11	CrO_4	CrO_4[a]
	Al_2O_3	8	CrO_4	CrO_4,[a] Cr_2O_7
	TiO_2	6	CrO_4,[a] Cr_2O_7	CrO_4, Cr_2O_7[a]
	ZrO_2	6	CrO_4,[a] Cr_2O_7	CrO_4, Cr_2O_7[a]
	SiO_2	2–4	CrO_4, Cr_2O_7[a]	Cr_2O_7, Cr_3O_{10},[a] Cr_4O_{13}
MoO_3	MgO	11	MoO_4	MoO_4
	Al_2O_3	8	MoO_4	MoO_4, Mo_7O_{24}, Mo_8O_{26}[a]
	TiO_2	6	MoO_4,[a] Mo_7O_{24}, Mo_8O_{26}	MoO_4, Mo_7O_{24},[a] Mo_8O_{26}
	ZrO_2	6	MoO_4,[a] Mo_8O_{26}	Mo_7O_{24}, Mo_8O_{26}[a]
	SiO_2	2–4	MoO_4, Mo_7O_{24},[a] Mo_8O_{26}	Mo_7O_{24}[a]
WO_3	MgO	11	WO_4	WO_4
	Al_2O_3	8	WO_4	WO_4, $W_{12}O_{39}$[a]
	TiO_2	6	WO_4,[a] $W_{12}O_{39}$	WO_4, $W_{12}O_{39}$[a]
	ZrO_2	6	WO_4,[a] $W_{12}O_{39}$	WO_4, $W_{12}O_{39}$[a]
	SiO_2	2–4	WO_4, $W_{12}O_{39}$[a]	$W_{12}O_{39}$[a]
Re_2O_7	MgO	11	ReO_4	ReO_4
	Al_2O_3	8	ReO_4	ReO_4
	TiO_2	6	ReO_4	ReO_4
	ZrO_2	6	ReO_4	ReO_4
	SiO_2	2–4	ReO_4	ReO_4

[a] Major species.
[b] Decavanadate-like environment.

solutions (Mo_7O_{24} and Mo_8O_{26} vs. W_6O_{21} and $W_{12}O_{39}$). The surface molybdenum and tungsten oxide species present on the hydrated oxide supports are in accordance with the trend predicted from the IEP values of the supports.

This approach can also be verified for CrO_3 species supported on a series of SiO_2·Al_2O_3 supports with increasing SiO_2 content under hydrated conditions, and the molecular structures have been determined with RS, EXAFS-XANES, and DRS [39]. The main results of this spectroscopic characterization are schematically illustrated in Figure 10. At low CrO_3 loadings, CrO_4 is the dominant species on Al_2O_3, whereas Cr_2O_7 species are present on a SiO_2 surface. Furthermore, the $[CrO_4]$:$[Cr_2O_7]$ ratio increases with increasing Al_2O_3 content of a SiO_2·Al_2O_3 support, and correspondingly the IEP of the SiO_2·Al_2O_3 support gradually increases. Higher CrO_3 loadings lead to the formation of Cr_2O_7 species even at an alumina support, whereas on a silica surface trichromates and tetrachromates were observed with RS. Thus, a general model has been developed that allows prediction of the molecular structures of surface metal oxide species on oxide supports under ambient conditions.

The presence of surface impurities or chemical promoters can also influence the molecular structure of surface metal oxides on hydrated surfaces since their presence should change the IEP of the oxide support [38]. Basic impurities will increase the pH of the thin film covering the surface of the oxide support, whereas acidic impurities will have the opposite effect. This effect has been observed for V_2O_5/TiO_2 and V_2O_5/Al_2O_3 catalysts contaminated with alkaline impurities, namely Na^+ and K^+. The presence of these impurities leads to the formation of surface othovanadate species rather than surface metavanadate and decavanadate species.

4.2. Catalyst Calcination

Heating freshly prepared or hydrated supported metal oxide catalysts in air or oxygen results in a gradual removal of the water molecules adsorbed on the catalyst material. The dehydrated metal oxide oxide species formed is oxidized to its highest oxidation state, and these species will anchor to the support surface via an esterification reaction with the hydroxyl groups of the amorphous oxide, resulting in the formation of

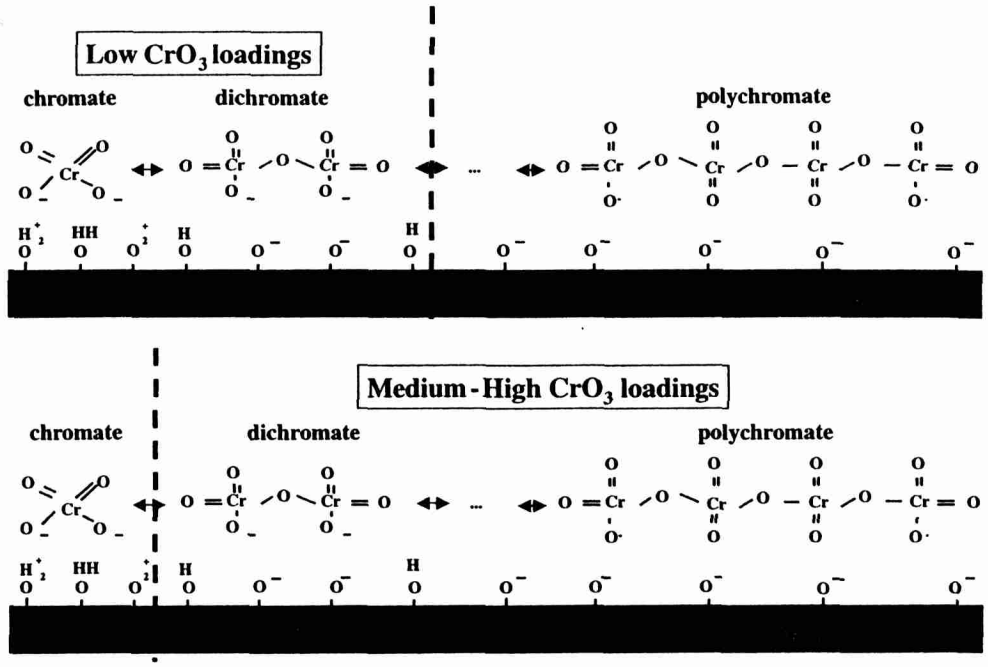

ig. 10. The molecular structures of hydrated supported chromium oxide catalysts as a function of the CrO_3 loading and SiO_2 content of a SiO_2·Al_2O_3 support. he polymerization degree of CrO_3 increases with increasing CrO_3 loading and SiO_2 content of the support.

ırface metal oxide species [19]. This is schematically drawn ı Figure 11 for a CrO_3/Al_2O_3 catalyst. Direct evidence for ıis anchoring reaction comes from IR indicating the con-ımption of hydroxyl groups, and this consumption is propor-onal to the quantity of deposited metal oxide. Turek et al. ave shown that on an alumina surface this reaction starts from ıe more basic hydroxyl groups and goes to the more acidic roups, indicating a kind of acid–base reaction between the ıetal oxide and the oxide support [40, 41]. In this respect, it striking that V_2O_5, for example, is much more difficult to isperse on a silica surface, especially at high V_2O_5 loadings. his is due to the relative inertness of the hydroxyl groups of ıe SiO_2 support. This results in the formation of microcrys-ıllites of V_2O_5 at the SiO_2 surface.

Elucidating the exact molecular structures of these sup-ɔrted metal oxides in the dehydrated state has been a sci-ıtific challenge for years [42, 43]. More specifically, it has been unknown, for example, how many terminal M=O bonds are present in these surface molecular species under dehydrated conditions. Thus, the question was whether the supported metal oxides were present as mono-oxo (one terminal M=O bond and three single M-O bonds), di-oxo (two terminal M=O bonds and two single M-O bonds) or tri-oxo species (three terminal M=O bonds and one single M-O bond). These three possibilities are shown in Figure 12 for a V_2O_5/TiO_2 catalyst.

To illustrate the lack of knowledge about dehydrated supported metal oxides, we can refer to the molecular structure of supported rhenium oxide catalysts, which have always been considered to consist of an isolated tri-oxo species of the type S-O-Re(=O)$_3$ species, where S represents a cation

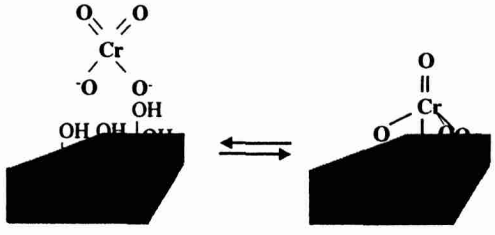

g. 11. Esterification reaction between the surface hydroxyl groups of a $_2O_3$ support and CrO_3 during calcination. This process is completely ersible, and rehydration of a calcined CrO_3/Al_2O_3 catalyst results in the rmation of a chromate species in the thin aqueous film covering the alumina pport.

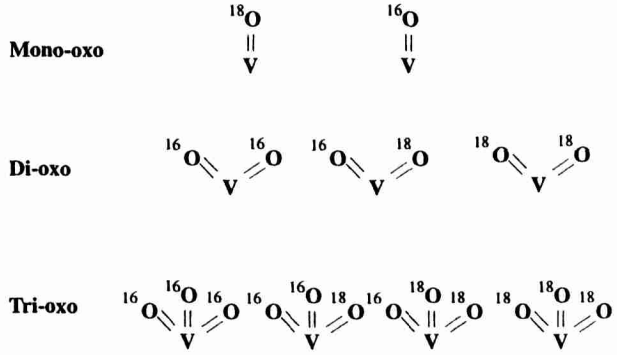

Fig. 12. Molecular models of mono-oxo, di-oxo, and tri-oxo surface vanadium oxide species on a support surface after calcination. The different molecular structures, which can be obtained after $^{18}O_2$ isotopic labeling, are also included. (Copyright 2000 American Chemical Society.)

of the support [35]. This surface species with three terminal Re=O bonds and one Re-O bond was proposed because it was assumed that the molecular structure of the freshly prepared or hydrated catalysts and those obtained after calcination were not really different. This observation was also confirmed by *ex situ* spectroscopic studies [38].

However, *in situ* RS, in combination with oxygen-18 isotopic labeling studies, have clearly shown that this assumption is not correct and that the molecular structure of supported metal oxide catalysts is drastically changed by drying and calcination of the hydrated catalyst material [44]. The different molecular structures possible after oxygen-18 isotopic labeling of supported metal oxide catalysts are also given in Figure 12. It has been shown that V^{5+}, Mo^{6+}, Nb^{5+}, W^{6+}, Cr^{6+}, and Re^{7+} oxides are all present as mono-oxo species on a zirconia support, and it is anticipated that the same molecular structures exist on other amorphous supports [42, 43]. This important conclusion indicates that the molecular structures of metal oxides are drastically restructered during the dehydration process (Fig. 11) and that *ex situ* spectroscopic measurements are of very little value for investigating metal oxide catalysts under realistic conditions. This observation seems to be valid not only for supported transition metal oxides but also for sulfates, for example. Indeed, the mono-oxo structure has also been revealed by IR and oxygen-18 isotopic exchange experiments for SO_4/Al_2O_3 and SO_4/TiO_2 [45].

Another scientific question is whether the supported metal oxide species are present as either a distorted monomeric or polymeric species. This question has also been resolved for many metal oxide catalyst systems by measuring *in situ* Raman spectra after different reduction treatments with either alkanes or methanol. It has been shown that in the case of supported chromium oxide catalysts, for example, both distorted polymeric and monomeric chromium oxide species are present on the surface of amorphous supports and the ratio of polymeric over monomeric species increases with increasing chromium oxide loading [46]. In addition, the polymeric chromium oxide species is more easily reduced at high temperatures than the isolated mono-oxo chromium oxide species. Based on all of these spectroscopic data, one can propose schematic drawings of the molecular structures of CrO_3, MoO_3, Nb_2O_5, WO_3, V_2O_5, and Re_2O_7 present at high metal oxide loadings on, for example, a zirconia support under dehydrated conditions [42, 43]. This is given in Figure 13. Similar drawings on the molecular structure can be made for the same metal oxides supported on other amorphous oxides, with the exception of a silica support, which behaves differently, as will be discussed in what follows.

Application of the mentioned methodology has made it possible to extract detailed information about the molecular structures of, for example, surface vanadium oxide species under hydrated conditions as a function of the support type (Al_2O_3, TiO_2, CeO_2, Nb_2O_5, ZrO_2, and SiO_2) and the V_2O_5 loading. In what follows, we will give a brief summary of the spectroscopic information obtained and the consequences for the molecular structure of the surface vanadium oxide species

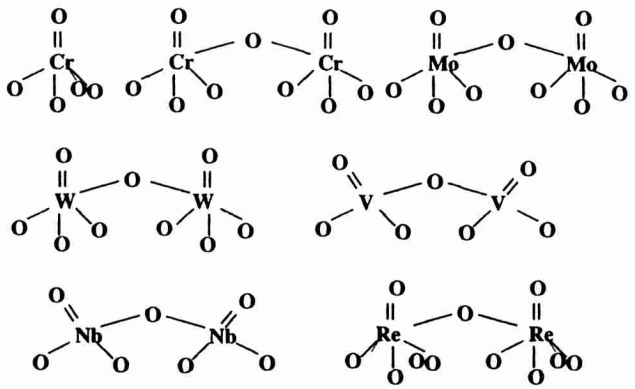

Fig. 13. Schematic drawing of the molecular structures of CrO_3, MoO_3, Nb_2O_5, WO_3, V_2O_5, and Re_2O_7 present on zirconia surfaces under dehydrated conditions at high metal oxide loadings. (Copyright 2000 American Chemical Society.)

[47] (Fig. 14). The calcined supported vanadium oxide catalysts with low V_2O_5 loadings have been shown to consist of VO_4 units possessing a mono-oxo V=O bond and three bridging V-O-S support bonds, and the supported vanadium oxide is fully oxidized to V^{5+}. On Al_2O_3, TiO_2, CeO_2, Nb_2O_5, and ZrO_2 supports this monovanadate species is characterized by a RS band at 1030 cm^{-1}, its exact position depending on the type of support. This band is assigned to the symmetric stretching mode of the terminal V=O bond. At higher V_2O_5 loadings, another broad and weak band appears in the Raman spectra, which is assigned to polymerized V-O-V stretching modes. By using the V=O stretching frequencies and the bond length correlation method developed by Hardcastle and Wachs for vanadia compounds [48], it was calculated that there are only very small differences in the bond lengths of the terminal V=O bond on the various amorphous supports (± 0.01 Å across the CeO_2, Al_2O_3, TiO_2, Nb_2O_5, ZrO_2 supports). The density of surface vanadium oxides is also the

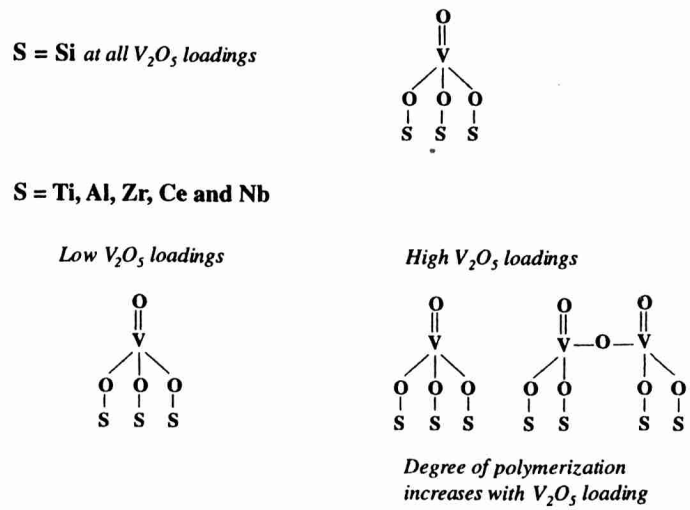

Fig. 14. Overview of the molecular structures of supported vanadium oxide catalysts under dehydrated conditions as a function of the support type and the vanadium oxide loading.

same on all of these supports at monolayer coverage (~8 V atoms/nm^2). Monolayer coverage is defined as the highest vanadium oxide loading that produces only surface VO_4 species and not V_2O_5 microcrystallites. Specific monolayer coverages, of course, are dependent on the surface area of the support: 3 wt% V_2O_5 on CeO_2. Thus, the molecular structures of supported vanadium oxide catalysts are almost independent of the support type.

This is not the case for V_2O_5/SiO_2 catalysts. Here, the chemical inertness of the SiO_2 supports results in a weak dispersion of V_2O_5, and V_2O_5 microcrystallites are easily formed on this support. Previously, only about 3 wt% V_2O_5 could be dispersed on a SiO_2 support, whereas Gao et al. have shown that highly dispersed V_2O_5/SiO_2 catalysts can also be prepared by a different synthesis method [49]. These authors were able to obtain a much higher V_2O_5 coverage of about 12 wt%. This surface coverage corresponds to a density of the surface vanadia sites of 2.6 V atoms/nm^2 on a 300 m^2/g SiO_2 support. Here, only monovanadate species with a mono-oxo V=O bond could be detected, as the only Raman band observed is the one at 1038 cm^{-1} and no bridging V-O-V modes could be spectroscopically revealed. The isolated nature of the surface vanadium oxides on SiO_2 at all loadings is unique to the silica support, although essentially the same molecular structure as the isolated vanadium oxide species is present on the other supports, at least for low V_2O_5 loadings. The only difference is the terminal V=O bond, which is somewhat shorter for V_2O_5/SiO_2 because it has a higher Raman stretching frequency. An overview of the molecular structures of supported vanadium oxide catalysts under dehydrated conditions as a function of the support type and vanadium oxide loadings is given in Figure 14 [47].

It is important to stress again that the molecular structures of supported metal oxides are clearly different in hydrated and dehydrated catalysts and that these structures can easily be interconverted by simply hydration and calcination [44]. These facts point to the very dynamic nature of supported metal oxides, as they readily respond to the environmental conditions by changing their molecular structures. This is futher illustrated in Figure 15 for supported MoO_3/SiO_2 catalysts, which undergo numerous structural transformations, depending on the temperature and reaction environment [50]. Under ambient conditions and at room temperature, the surface molybdenum oxide species are present as Mo_7O_{24} clusters. Additional moisture results in a transformation of the Mo_7O_{24} cluster into $H_4SiMo_{12}O_{40}$ or a silicomolybdic acid heteropolyoxoanion. These molybdate clusters are decomposed during calcination into an isolated surface molybdenum species with one terminal Mo=O bond and four bridging Mo-O-Si bonds. Exposure of this calcined supported metal oxide catalyst to a vapor containing methanol and oxygen results in the formation of crystalline β-MoO_3. These β-MoO_3 crystallites are not thermally stable and convert above 300°C to β-MoO_3 crystallites.

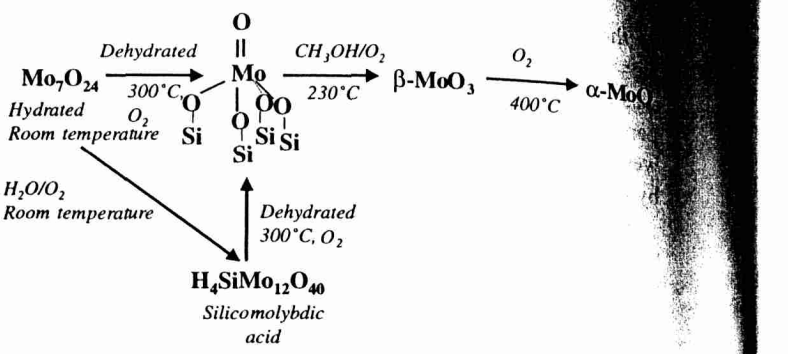

Fig. 15. Structural transformations taking place in a MO_3/SiO_2 catalyst as a function of the reaction temperature and reaction environment.

4.3. Catalyst Activation

Several factors influence the activation process of supported metal oxide catalysts, and, as an example, we will discuss first the activation of supported chromium oxide catalysts [51–54]. At the end of this section, we will discuss the different factors that influence the activation process of these catalysts. Supported chromium oxide catalysts are industrially used for the nonoxidative dehydrogenation of propane and isobutane to propene and isobutane, respectively (mainly by CrO_3/Al_2O_3 catalysts), and for the polymerization of ethylene to high-density polyethylene (HDPE) or linear low-density polyethylene (LLDPE) (mainly by CrO_3/SiO_2) [17, 21, 22]. These supported metal oxide catalysts are, however, not catalytically active directly after the calcination treatment in an oxygen-rich environment. Instead, the supported chromium oxides have to be first reduced at relatively high temperatures to a lower oxidation state to become active in one of the mentioned catalytic processes.

This activation process can be studied by applying a combination of ESR and DRS. ESR allows quantification of the amount of Cr^{5+} and, to a lesser extent, of Cr^{3+} species on the catalyst surface after calcination and after different reduction steps [51–54]. The amount of Cr^{6+}, Cr^{3+}, and Cr^{2+} species on support surfaces can be quantified after such pretreatments with DRS. This spectroscopic approach is applicable to CrO_3/Al_2O_3, CrO_3/SiO_2, and $CrO_3/SiO_2 \cdot Al_2O_3$ catalysts with different Al_2O_3 contents, at least for low chromium oxide loadings. Indeed, combined DRS-ESR spectroscopies have shown that

1. Cr^{6+} is the dominant species on the surface of amorphous supports after calcination for supported chromium oxide catalysts with a low CrO_3 loading, whereas Cr^{5+} species are always present in trace amounts.
2. The reduction of supported Cr^{6+} and Cr^{5+} species on an alumina support with CO starts above 200°C, and these species are gradually converted mainly to Cr^{3+} and Cr^{2+}. However, the amount of Cr^{2+} is always limited and small in comparison with Cr^{3+}. Figure 16 shows the relative changes of the amount of Cr^{6+},

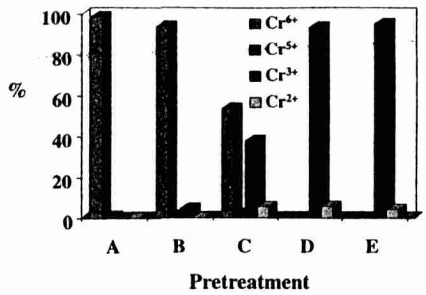

Fig. 16. Distribution of Cr^{6+}, Cr^{5+}, Cr^{3+}, and Cr^{2+} on an Al_2O_3 support for a 0.2 wt% CrO_3/Al_2O_3 catalyst as a function of the pretreatment. (A) Calcination at 550°C. (B) Reduction with CO at 200°C. (C), Reduction with CO at 300°C. (D) Reduction with CO at 400°C. (E) Reduction with CO at 600°C. (Copyright 1999 Elsevier Science BV.)

Cr^{5+}, Cr^{3+}, and Cr^{2+} in a 0.2 wt% CrO_3/Al_2O_3 catalyst with increasing reduction temperature between 200 and 600°C.

3. Comparison between different amorphous supports indicates that the $[Cr^{2+}]$:$[Cr^{3+}]$ ratio increases with increasing SiO_2 content of the support. Thus, SiO_2-rich supports prefer Cr^{2+} ions, whereas on alumina mainly Cr^{3+} is present, and all of these spectroscopic observations are in line with TPR and EXAFS-XANES measurements on the same set of Cr-based catalysts. Thus, an average oxidation state of 2 and 3 was obtained after reduction with CO for CrO_3/SiO_2 and CrO_3/Al_2O_3 catalysts, whereas $CrO_3/SiO_2 \cdot Al_2O_3$ catalysts have an intermediate average oxidation state. The average oxidation state of Cr after CO reduction gradually increases with increasing Al_2O_3 content of the $SiO_2 \cdot Al_2O_3$ support.

It is also important to notice that the combined DRS-ESR approach has been extended to supported vanadium oxide catalysts [55] and to chromium oxides dispersed on the surface of zeolites [54]. In the latter case, useful information about the redox behavior of Cr^{6+} in a series of zeolites differing in their chemical composition and framework type (namely, zeolite Na-X, zeolite Na-Y, zeolite H-Y, Ga-containing zeolite Na-Y, and Na-mordenite) could be revealed by monitoring the amount of Cr^{6+} as a function of the reduction temperature in the presence of CO. It was concluded that

1. CO reduction of CrO_3 dispersed on the surfaces of zeolites starts above 200°C.
2. The amount of Cr^{6+} species at the zeolite surface is zero after reduction at 600° C, except for a CrO_3/zeolite H-Y zeolite prepared via the solid-state ion exchange procedure with a $CrCl_3$ salt ($CrCl_3 + H\text{-}Y \rightarrow Cr/H\text{-}Y + 3HCl \uparrow$).
3. The relative decrease in the amount of Cr^{6+} species in the region 200–600°C, when used as a reducibility criterion, follows the sequence CrO_3/zeolite Y (prepared via solid-state ion exchange) < CrO_3/zeolite Ga-Y (prepared via ion exchange) < CrO_3/zeolite X (prepared via ion exchange) < CrO_3/zeolite Y (prepared via ion exchange) < CrO_3/zeolite Y (prepared via impregnation) < CrO_3/mordenite (prepared via ion exchange).

These observations reinforce the general idea that both the chemical composition of the support and the preparation method of the catalytic material have a strong influence on the chemical properties of supported metal oxides.

One can also obtain information about the reduction kinetics of supported chromium oxide catalysts by monitoring the amount of Cr^{6+} on a catalyst surface during a CO reduction process by using *in situ* DRS spectroscopy [56, 57]. It was found that the amount of Cr^{6+} follows a two-exponential decay for both CrO_3/SiO_2 and CrO_3/Al_2O_3 catalysts, but the decay is much faster for a SiO_2 than for an Al_2O_3 support. The following reaction scheme can explain the data:

$$Cr_a + CO \rightarrow Cr_a(CO)_{ads} \rightarrow Cr^{m+}(CO_2)_{ads} \rightarrow Cr^{m+} + CO_2 \ (\text{with } m < 6) \qquad (4)$$

with Cr_a, an anchored Cr^{6+} species. The rate-determining step is the reduction of Cr^{6+} by CO with formation of carboxylates, which decompose to CO_2. The rate constant is one to two orders larger for CrO_3/SiO_2 than for CrO_3/Al_2O_3. This may have to do with differences in dispersion, a much stronger interaction of Cr^{6+} species with an alumina than with a silica surface, and a better stabilization of the Cr^{3+} and Cr^{5+} species on alumina after reduction with CO.

A comment also has to be made about the factors influencing the activation process of supported metal oxide catalysts. In particular, it is important to know which parameters are influencing the final oxidation state of the different metal oxide species present in supported metal oxide catalysts after a particular reduction treatment. At least six parameters have a direct influence on this reduction process, although it is very difficult to really discriminate between the different parameters in a particular reduction treatment.

1. The calcination treatment. A higher calcination temperature of the catalyst generally results in a lower mean average oxidation state of the supported metal oxides after reduction. This lower average oxidation state is related to the dehydroxylation degree of supports, such as alumina and silica. Surface hydroxyl groups of these supports can be removed by calcination, as it is known that surface hydroxyl groups, and, in particular, surface acidity, retard the reduction of supported metal oxides. This explains, for example, the severe reduction conditions of Cr^{6+} in a CrO_3/H-Y zeolite because only a small number of hydroxyl groups have been replaced by $CrCl_3$ during the solid-state ion exchange process [54]. Another effect of the surface hydroxyl groups is, of course, that these groups can partially coordinate to the reduced metal ion, giving rise to a different coordination environment. This can influence, for example, the polymerization activity of CrO_3/SiO_2 catalysts [21, 22].

2. The chemical composition of the support. The harder the support, the less susceptible the structure of the oxide support is to electron fluctuations. Such electron fluctuations are necessary for a reduction process. Thus, the harder the support, the more difficult the reduction will be. The chemical hardness of an inorganic support increases when, for example, (a) the aluminum content increases in a silicium type of support and (b) aluminum is changed by a harder atom, such as Ga. These differences can partially explain the differences in redox behavior of Cr observed in Cr-containing zeolites. Indeed, the chemical hardness increases from CrO_3/Na-mordenite over CrO_3/Na-Y and CrO_3/Na-X to CrO_3/Ga-containing Na-Y. The reduction behavior of surface Cr^{6+} species follows the reverse order, as was predicted [54].

3. The support type. Supported metal oxides are more difficult to reduce in zeolites in comparison with amorphous supports. This difference must be related to the accessibility of the supported metal oxide by the reducing agent. Figure 17 shows the difference in redox behavior between Cr^{6+} dispersed in CrO_3/Al_2O_3 and CrO_3/Na-Y catalysts [54]. This figure shows that the reduction of Cr^{6+} at 380°C is much faster in a CrO_3/Al_2O_3 material in comparison with a CrO_3/Na-Y material reduced with CO at 410°C. The reduction of Cr^{6+} in a CrO_3/Na-Y catalyst is only partial at 410°C, and higher reduction temperatures are necessary for a complete reduction of Cr^{6+} to $Cr^{3+/2+}$ species.

4. The degree of dispersion of the supported metal oxide. As a general rule one can state that the larger the supported metal oxide cluster, the more easily it can be reduced. Thus polymeric metal oxide species are more easily reducible than monomeric metal oxide species. Because the relative amount of polymeric supported metal oxide species increases with increasing metal oxide loading, the supported metal oxide catalysts are the most difficult to be reduced at low metal oxide coverages. An example is the difference in redox properties of surface polychromates and monochromates. A surface monochromate species is more difficult to reduce than a surface polychromate species, and thus the temperature at which the surface metal oxides starts to be reduced shifts to lower values with increasing metal oxide loadings [19]. Related to this difference in metal oxide dispersion is the change in the dispersion of supported metal oxide during a reduction treatment. An illustrating example is the V_2O_5/SiO_2 catalysts, as shown in Figure 18 [58]. Reduction results in the removal of oxygen atoms from the supported vanadium oxide species, and at high V_2O_5 loadings the reduced species have the tendency to interact with a neigboring surface vanadium site by sharing oxygen atoms. This interaction is only possible at high V_2O_5 loadings because the average distance between the vanadium sites is rather low and thus favors interactions between them. This results in the formation of microcrystalline V_2O_5 particles.

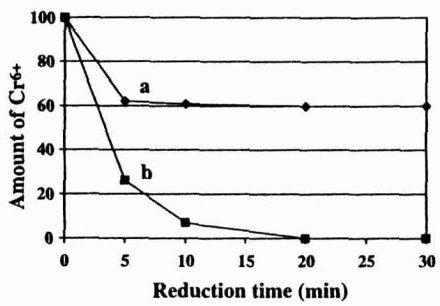

Fig. 17. Amount of Cr^{6+} as a function of time for (a) a CrO_3/Na-Y zeolite reduced with CO at 410°C and (b) a CrO_3/Al_2O_3 catalyst reduced with CO at 380°C.

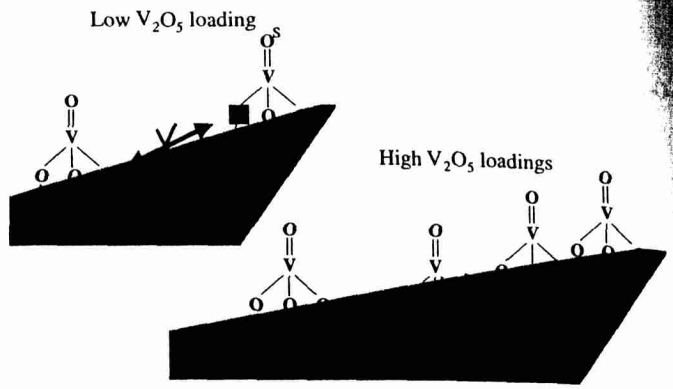

Fig. 18. Change in dispersion during a reduction treatment for a V_2O_5/TiO_2 catalyst.

5. The reducing agent. Diluted gas streams of CO and H_2 are frequently used to activate supported metal oxide catalysts, although the reducing properties of the surface metal oxides are clearly different, depending on the presence of either CO or H_2. In the case of supported chromium oxide catalysts, CO reduction results in a deeper reduction as compared with H_2 reduction for the same reduction temperature [59]. Thus, the $[Cr^{2+}]$:$[Cr^{3+}]$ ratio on a reduced alumina or silica surface is higher when the supported metal oxide catalyst is reduced with CO instead of H_2. An explanation for this difference can be the production of H_2O during the reduction with H_2, as it is known that Cr^{2+} is rather unstable in the presence of H_2O and is readily reoxidized to Cr^{3+}.

6. The type of supported metal oxide. The differences between the reducing agents cannot be extended to other supported metal oxide catalysts. For example, reduction profiles for supported vanadium oxide catalysts show that the average oxidation state of surface vanadium oxides after reduction is higher in the case of CO than in the case of H_2. Additional XPS measurements have shown that V^{4+} species are more stabilized on the catalyst surface if CO is used as a reducing agent. Thus, the final oxidation state of the surface metal oxide after reduction is also dependent on the particular metal ion supported on an inorganic oxide.

4.4. Catalysis: Active Sites and Reaction Intermediates

Although many catalytic reactions have been studied in detail by different characterization techniques, the selective oxidation of methanol to formaldehyde over supported vanadium

oxide catalysts is a particularly useful example because this catalytic reaction can be considered as a simple probe reaction for other selective oxidation reactions as well [60]. Examples of such oxidation reactions are the selective oxidation of butane to maleic anhydride and *o*-xylene to phthalic anhydride and the oxidative dehydrogenation of propane and butane to propene and butene, respectively. As a consequence, the concepts developed for the selective oxidation of methanol over supported vanadium oxide catalysts can easily be transferred to these catalytic reactions as well.

The selective oxidation of methanol can be written as

$$CH_3OH + O_2 \rightarrow CH_2O + H_2O \qquad (5)$$

and is conducted over supported metal oxide catalysts at 230°C in a fixed-bed reactor. During the oxidation of methanol to formaldehyde over supported vanadium oxide catalysts, the surface vanadium oxide species on the surface of amorphous supports becomes partially reduced by the reaction environment [36, 37, 47, 50, 60]. *In situ* RS has revealed that during methanol oxidation the V^{5+} species retained its molecular structure and that these species are partially reduced to lower oxidation states. RS shows a 40–60% reduction of the intensity of the Raman signal, indicating that some V^{5+} is reduced to $V^{4+/3+}$. The latter species were detected with *in situ* DRS, at least in the case of V_2O_5/Al_2O_3 and V_2O_5/TiO_2 catalysts. No reduction to $V^{4+/3+}$ could be observed for V_2O_5/SiO_2 catalysts measured under reaction conditions. The actual extent of this reduction is thus certainly lower because RS cannot be used in a quantitative way, and the DRS spectra are not of sufficient quality to get quantitative information about $V^{4+/3+}$ species. In any case, the extent of reduction during methanol oxidation is rather limited and was almost independent of the surface coverage of the surface vanadia oxides, the specific support type, and the reaction temperature. This suggests that the fraction of surface vanadia species participating in this oxidation reaction is almost constant. In addition, *in situ* IR spectroscopy during methanol oxidation revealed the presence of a surface methoxy intermediate species.

Catalytic measurements show that the selectivities to formaldehyde were 90–99% for V_2O_5/TiO_2, V_2O_5/ZrO_2, V_2O_5/Nb_2O_5, and V_2O_5/CeO_2 catalysts, whereas only a selectivity of 50% to formaldehyde was observed for a V_2O_5/Al_2O_3 catalyst [47]. The major unselective product was dimethyl ether, which is associated with the presence of some surface acid sites at the catalyst surface. The relative independence of the turnover frequency (TOF), which is defined as the number of methanol molecules converted per surface vanadia site per second, with the surface vanadia loading at each of the amorphous supports, indicates that the reaction rate is first order with respect to the surface vanadia sites. This suggests that the oxidation of methanol to formaldehyde over supported vanadium oxide catalysts is a unimolecular reaction requiring only one surface vanadia species, which can be referred to as the catalytically active site. A possible reaction mechanism is given in Figure 19, showing the presence of a spectroscopically observed reaction intermediate, namely the V-O-CH_3 species [60]. It shows a two-step process, in which first the methanol molecule is chemisorbed onto a surface vanadia species with the formation of a methoxy group. In a second step, formaldehyde and water are desorbed from the catalyst surface. Molecular oxygen is required in this step to reoxidize the reduced vanadium site to V^{5+}.

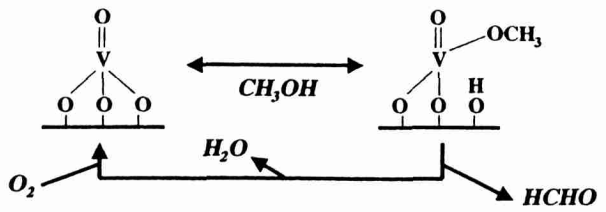

Fig. 19. Reaction scheme for the selective oxidation of methanol to formaldehyde over supported vanadium oxide catalysts. The reaction mechanism consists of two steps, in which a surface methoxy intermediate species is formed and experimentally detected by *in situ* spectroscopy.

The scheme in Figure 19 is a typical example of the Mars–Van Krevelen redox mechanism, in which the oxidation of hydrocarbons proceeds by two steps. In a first step, the reactant hydrocarbon molecule initially reduces the oxidized surface site, whereas the reduced surface site is subsequently reoxidized with gas-phase molecular oxygen in a second step. This is indeed experimentally observed for the oxidation of methanol to formaldehyde over supported vanadium oxide catalysts. It implies that the reactivity properties have to be explained solely in terms of differences in structural properties of the dehydrated surface vanadia species (V^{5+}) and not in terms of differences in the molecular structures of reduced V^{3+} and V^{4+} species. One of the intriguing questions for years was then which molecular bond in the surface vanadium oxide species is responsible for the catalytic activity of these catalysts in selective oxidation reactions [61–63]. Three types of bonds, can be distinguished: terminal V=O bonds, bridging V-O-V bonds, and V-O support bonds (Fig. 6). In what follows, we discuss the experimental evidence currently available to evaluate the possible role of each of these bonds in the selective oxidation of methanol:

1. Role of terminal V=O bonds. Many investigators have been convinced that this bond contains the oxygen critical for selective oxidation reactions. However, *in situ* Raman spectroscopy in combination with catalytic measurements has shown that there is no relation between the terminal V=O bonds and the catalytic performances of supported vanadium oxide catalysts. Indeed, the TOF was found to vary drastically, although identical V=O Raman features were observed for these catalysts. This is shown in Table VI for the selective oxidation of methanol to formaldehyde, and similar results were obtained for the oxidation of butane to maleic anhydride. Furthermore, oxygen-18 labeling of the terminal V=O bond during butane oxidation and methanol oxidation revealed that this bond is very stable and has an exchange time that is approximately 20 times longer than the characteristic reaction time. A series of *in situ* Raman spectra at different degrees of

Table VI. Catalytic Performances and Raman Frequency of the V=O Bond for a Series of Supported Vanadium Oxide Catalysts [47, 50]

Supported vanadium oxide catalysts	TOF at 230°C	V=O bond (cm^{-1})
V_2O_5/CeO_2	$\sim 1 \times 10^1$	1028
V_2O_5/TiO_2	$\sim 1 \times 10^0$	1030
V_2O_5/ZrO_2	$\sim 2 \times 10^0$	1030
V_2O_5/Nb_2O_5	$\sim 4 \times 10^{-1}$	1033
V_2O_5/Al_2O_3	$\sim 7 \times 10^{-2}$	1026

oxygen-18 labeling is given in Figure 20. It is shown that the $V=^{18}O$ bond is gradually transformed into a $V=^{16}O$ bond during methanol oxidation, but with an exchange rate much slower than the effective reaction rate. All of these experimental observations strongly suggest that the terminal V=O bonds do not contain the critical oxygen that is involved in selective oxidation reactions.

2. Role of bridging V-O-V bonds. It was already discussed that the ratio of polymerized to isolated surface vanadia species increases with increasing vanadia loading, with the exception of V_2O_5/SiO_2 catalysts. Evidence for this comes from *in situ* Raman and DRS spectroscopies. As a consequence, the surface concentration of bridging V-O-V bonds increases with increasing vanadia loading. The TOF of these catalysts, however, is independent of the vanadia loading, as shown in Figure 21. This indicates that the oxygen associated with the V-O-V bond does not critically participate in the oxidation reaction.

3. Role of V-O-support bonds. Unfortunately, the role of this bond cannot be directly assessed because no spectroscopic technique is currently available to characterize the V-O support bond. Therefore, only indirect information can be obtained by changing the specific support composition, for example.

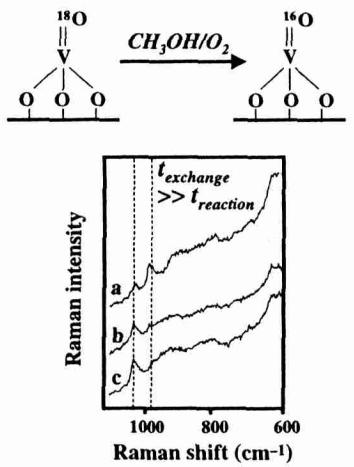

Fig. 20. *In situ* Raman spectra during the selective oxidation of methanol to formaldehyde over a V_2O_5/ZrO_2 catalyst. The supported metal oxide catalyst was first partially transformed with $^{18}O_2$ in its ^{18}O form by a reduction–reoxidation treatment with *n*-butane and oxygen-18. Repeating this reduction–reoxidation cycle for several times results in a shift of the 1030 cm^{-1} Raman band to approximately 1000 cm^{-1}.

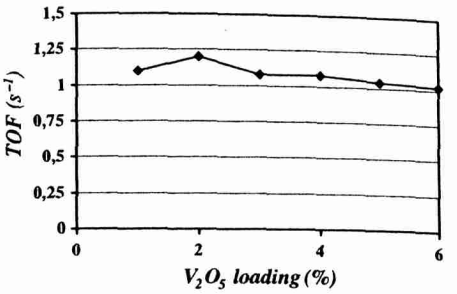

Fig. 21. TOF values of a V_2O_5/ZrO_2 catalyst as a function of the V_2O_5 loading in the selective oxidation of methanol to formaldehyde reaction at 230°C.

This is possible without significantly changing the molecular structures of the supported vanadium oxide species for ZrO_2, TiO_2, Nb_2O_5, and Al_2O_3 as supports. Since changing the specific oxide composition dramatically influences the TOF of the corresponding supported vanadium oxide catalysts for the selective oxidation of methanol, it strongly suggests that the oxygen in the V-O support bond is critical for this catalytic reaction.

Finally, an interesting phenomenon is taking place during the selective oxidation of methanol to formaldehyde when bulk metal oxides, such as CrO_3, MoO_3, V_2O_5, Re_2O_7, and Cr_2O_3, are deposited on the surface of oxide supports via physical mixing [64, 65]. The metal oxides are spread on the surface of the supports during the selective oxidation reactions with the formation of a two-dimensional overlayer of supported metal oxides. Furthermore, this phenomenon also takes place for other alcohol molecules. This reaction-induced spreading is a new phenomenon, which takes place at temperatures much lower than required for thermal spreading and results in the formation of a two-dimensional metal oxide species on the surface of oxide supports starting from three-dimensional bulk metal oxides. Thermal spreading is a spontaneous process from the thermodynamics point of view, which is well documented in the catalysis literature. The driving force of this spreading process is the decrease of the overall system surface free energy, and its kinetics is limited because of the high temperatures required for the surface diffusion and migration of the metal oxide over the surface of the oxide support. In the context of thermal spreading, the Tamman temperature is often used to estimate the temperature for thermal treatments. The Tamman temperature in the case of MoO_3, for example, is 261°C, and higher temperatures are required to have bulk MoO_3 crystallites spreading onto an oxide support at an appreciable rate. Reaction-induced spreading, on the other hand, takes place at temperatures lower than the Tamman temperature of the specific bulk metal oxide. This temperature is the reaction temperature of 230°C in the case of the selective oxidation of methanol to formaldehyde.

Wachs et al. have recently shown that reaction-induced spreading is taking place for CrO_3, MoO_3, V_2O_5, Re_2O_7, and Cr_2O_3 on TiO_2 and SnO_2 supports, but not on SiO_2 supports

because of the small interaction between this support and metal oxides [64, 65]. The mechanism of the reaction-induced spreading proceeds via the reaction of an alcohol with metal cations to form surface mobile and volatile metal-alkoxy complexes. The transport of these complexes takes place through surface diffusion and volatilization/readsorption. The kinetics of the spreading process is accelerated by the reaction temperature and is also dependent on the alcohol molecule. The rate of spreading decreases in the order methanol $\gg$ ethanol $>$ 2-butanol. The high reaction-induced spreading efficiency of methanol is related to the high volatility of the metal-methoxy complexes. The reaction-induced spreading also has a direct influence on the catalytic performances of such mixed metal oxide materials, since surface metal oxide species are much more active than bulk metal oxides for selective oxidation reactions. This is evident for a physical mixture of, for example, MoO_3 and TiO_2 exposed to methanol and oxygen at 230°C. In the beginning of the reaction the TOF is only 0.020, whereas after 400 min the TOF is increased to 0.040. This increase in catalytic activity is correlated with an increase in the number of surface metal oxide species at the oxide support.

4.5. Catalyst Deactivation

Deactivation of supported metal oxide catalysts can be due to several factors, but it is most frequently related to the unavailability of the active site for the reactant molecule. The three most common deactivation routes are

1. Formation of carbon deposits or coke. These deposits cover the catalyst surface and prevent the reactant molecule from reaching the active site of the supported metal oxide catalyst. An example is the gradual decrease in activity of Fe/H-ZSM-5 catalysts in the direct conversion of methane to aromatics due to the gradual formation of surface carbon deposits [20]. This deactivation process can be easily monitored with XPS by evaluating the C 1s binding energies of the carbon deposits formed.

2. Blocking of the pore system of supported metal oxides. This pore blocking is related to the formation of rather large organic molecules from the reactant molecule within the catalyst pores. This deactivation route is most frequently encountered when molecular sieves with active sites dispersed over the internal surface of the material are used as heterogeneous catalysts. The product molecules formed within the supercages of zeolite Y, for example, are too big to be released into the reaction mixture via the 12-membered oxygen rings of the supercage, and the zeolite catalyst will readily deactivate. Another example is the breaking up of the pore system of an amorphous silica particle during the polymerization of ethylene [21, 22]. If the silica structure is too rigid to break up into smaller parts, the polyethylene chain can no longer grow because ethylene molecules are not able to reach the catalytically active Cr centers.

3. Change in metal oxide dispersion. The active site of a catalyst can be either isolated or clustered, or a combination of both, but is always a surface species. Supported metal oxide catalysts are dynamic systems and readily respond to the reaction environment. This may result in a change in the di persion of the active site at the catalyst surface. An examp is the clustering of an isolated active site into a new clu tered metal oxide phase at the support surface and has alread been discussed for the reduction process of V_2O_5/SiO_2 ca alysts with a high V_2O_5 loading [49, 58]. The metal oxid clusters formed, *in casu* microcrystalline V_2O_5 oxides, mostl have a lower activity or may catalyze undesirable side reac tions. Another potential problem can be the migration of th surface species into a species incorporated into the lattice o the support. This process can be reversible or not, dependin on the type of support and the coordination requirements o the metal ion.

A first example is the formation of V^{3+} species when a V_2O_5/Al_2O_3 catalyst is exposed to a stream of *n*-butane molecules at high temperatures [66]. The overall result is the migration of this V^{3+} species into the lattice of alumina, where it will take an octahedral vacancy. This migration process is reversible, and reoxidation results in a reappearance of surface vanadia species.

Another illustrative example of an almost irreversible migration process is a CrO_3/Al_2O_3 catalyst used for the dehydrogenation of alkanes [17]. The severe catalytic conditions result in the formation of surface Cr^{3+} species, which are likely to migrate into empty octahedral vacancies of the alumina support. The catalyst is continuously cycled between the oxidized and reduced states and during each reduction step, part of the Cr^{3+} is migrating into the support lattice. The solid-state diffusion of Cr^{3+} ions into these vacant Al^{3+} sites is facilitated by the similar ionic radii and charge of Cr^{3+} and Al^{3+}. This migration process is visualized in Figure 22. It shows the amount of surface Cr^{6+} and incorporated Cr^{3+} as determined by DRS spectroscopy for a 0.5 wt% CrO_3/Al_2O_3 catalyst as a function of the number of reaction cycles. A typical reaction cycle consists of a calcination treatment at 700°C in the presence of oxygen for 15 minutes and a treatment with propane at 700°C for 15 minutes.

Figure 22 also shows that the calcined CrO_3/Al_2O_3 catalyst exclusively contains Cr^{6+} species and that the amount of these species gradually decreases with increasing number of catalytic cycles at the expense of the formation of pseudo-octahedrally coordinated Cr^{3+} species, which are located in the empty vacancies of the alumina support. Other evidence for this migration process comes from ^{27}Al magic angle spinning nuclear magnetic resonance (NMR) of deactivated CrO_3/Al_2O_3 catalysts, indicating that Cr^{3+} ions occupy sites in the close vicinity of octahedral Al^{3+} in the alumina matrix. This suggests that a type of Cr_2O_3-Al_2O_3 spinel structure is formed during the reduction–reoxidation cycling, which results in the irreversible deactivation of these alkane dehydrogenation catalysts. The result is that the catalyst is totally deactivated after 2 years in an industrial plant and has to be replaced with new catalyst material.

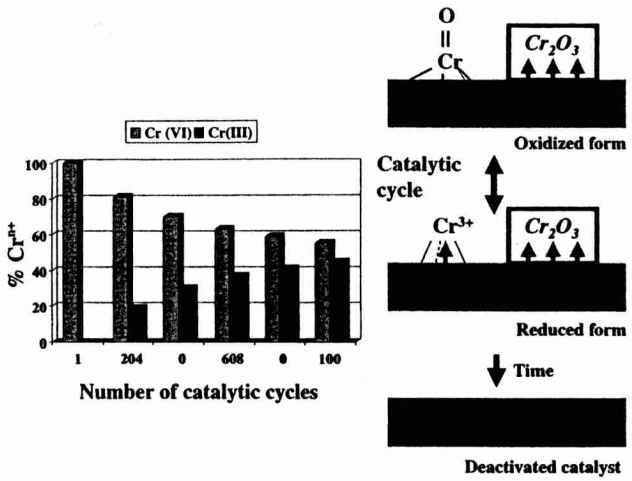

Fig. 22. Migration process of surface Cr ions into an Al_2O_3 support during catalyst cycling in an alkane dehydrogenation plant. This process takes place within about 2 years of catalyst operation. The left hand scheme shows the evolution of the amount of Cr^{6+} and Cr^{3+} with increasing number of catalytic cycles, and the right-hand scheme gives an illustration of the different processes taking place in the catalyst bed during an industrial operation.

5. CATALYSIS BY SUPPORTED METAL OXIDES

5.1. General Overview

Tables VII–XVIII give a general overview of all the catalytic applications of supported metal oxide catalysts. This rather exhaustive list of catalytic applications has been obtained from the Web of Science of the Institute of Scientific Information by using the key words "supported *x* oxide catalyst" or "supported *x* oxides," where *x* is titanium, vanadium, chromium, manganese, iron, cobalt, nickel, copper, molybdenum, tungsten, rhenium, or niobium [67–295]. They can be applied in

Table VII. Catalysis by Supported Titanium Oxides

Catalytic reaction	Reference
Photodecomposition of chlorinated phenols	67, 68
Photoreduction of carbon dioxide	69, 70
Photodecomposition of rhodamine-6G and phenol	71, 72
Complete photocatalytic oxidation of ethylene	73
Photooxidation of propane	74
Catalytic decomposition of 1,2-dichloroethane	75
Catalytic decomposition of freon-12	76
Catalytic decomposition of chloroform	77
Isomerization of 1-butene	78
Isomerization of methyloxane to propanal	79
Dehydration of methanol	80
Hydration of ethylene	81
Amination of phenol	81
Dealkylation of cumene	82
Hydrocracking of decane	83
Dehydration of propanol	84
Solvolysis of *cis*-2,3-epoxybutane	85
Ammoxidation of cyclohexanone	86
Epoxidation of α-isophorone by peroxides	87, 88
Epoxidation of olefins by peroxides	89–91
Selective oxidation of cyclohexane by peroxides	92
Hydroxylation of phenol by peroxides	93
Oxidation of benzene and toluene by peroxides	93
Oxidation of *n*-alkanes with peroxides	94
Oxidation of methanol to formaldehyde	95, 96
Transesterification of dimethylcarbonate and phenol	97
Ammoximation of cylcohexanone	98

Table VIII. Catalysis by Supported Vanadium Oxides

Catalytic reaction	Reference
Selective oxidation of alkanes and alkenes	99, 100
Selective catalytic reduction of NO_x with NH_3	101–103
Oxidation of *o*-xylene to phthalic anhydride	104, 105
Ammoxidation of aromatics and methylaromatics	106–108
Selective oxidation of methanol to formaldehyde	109
Oxidation of SO_2	110–112
Decomposition of isopropylalcohol	113
Oxidation of aliphatic and aromatic hydrocarbons	114, 115
Photooxidation of CO	116
Photoisomerization of butene	117
Partial oxidation of methane to formaldehyde	118–120
Oxidation of H_2S	121, 122
Synthesis of isobutyraldehyde from methanol and ethanol	123
Selective oxidation of 4-methylanisole	124
Selective oxidation of *p*-methoxytoluene	125
Alkylation of aldehydes with methanol	126
Oxidative coupling of CH_4	127
Synthesis of 2,6-dimethylphenol from methanol and cyclohexonane	128
Synthesis of isobutyraldehyde from methanol and *n*-propylalcohol/ethanol	129, 130
Total oxidation of benzene	131
Dehydrocyclodimerization of isobutene to xylene	132
Polymerization of olefins	133
Selective oxidation of alkanes with peroxides	134
Oxidative dehydrogenation of alkanes	135–137
Isomerization of *m*-xylene	138
Epoxidation of alkenes with peroxides	139
Hydroxylation of phenol	140
Direct conversion of CH_4 to aromatics	141, 142

Table IX. Catalysis by Supported Chromium Oxides

Catalytic reaction	Reference
Polymerization of ethylene	143, 144
Nonoxidative dehydrogenation of alkanes	145–147
Hydrogenation of alkanes	148, 149
Dehydrocyclization of alkanes	150
Selective Catalytic reduction of NO_x with NH_3	151
Selective oxidation of organics in the presence of peroxides	152–154
Selective oxidation of alkenes	155
Oxidation of CO	156
Isomerization of alkenes	157
Catalytic destruction of chlorinated hydrocarbons	158, 159
Selective oxidation of methanol	160
Selective oxidation of H_2S	161
Oxidative dehydrogenation of alkanes	162, 163
Selective oxidation of organics in the presence of oxygen	164
Dehydrogenation of ethane with CO_2	165
Synthesis of 2,6-demethylphenol from methanol, cyclohexanone, and cyclohexanol	166
Fluorination of 1,1,1-trifluoro-2-chloroethane	167
Direct conversion of CH_4 to aromatics	168, 169

Table X. Catalysis by Supported Manganese Oxides

Catalytic reaction	Reference
Oxidation of hydrocarbons	170
Catalytic combustion of CH_4	171
Decomposition of NO	172
Decomposition of O_3	173, 174
Selective catalytic reduction of NO_x with NH_3	175, 176
Dehydration of 2-propanol and methanol	177, 178
Oxidation of ethanol with O_3	179, 180
Selective oxidation of cyclohexene and styrene and with air	181
Oxidative dehydrogenation of ethane	182
Selective oxidation of cyclohexene, styrene, and *trans*- and *cis*-stilbene with peroxides	183–185
Oxidation of CO	186
Non-oxidative conversion of CH_4 to higher hydrocarbons	187
Oxidation of hydrocarbons and alcohols by CO_2	188
Decomposition of hydrogen peroxide	189

Table XI. Catalysis by Supported Iron Oxides

Catalytic reaction	Reference
Epoxidation of propene by NO	190
Partial oxidation of methanol	191
Combustion of CH_4	192
Dehydrogenation of ethylbenzene	193
Reduction of NO and N_2O by CO	194
Oxidative dehydrogenation of ethylbenzene with CO_2	195
Desulfurization of H_2S	196, 197
Oxidation of CO	198
Dehydrogenation of 1-butene and ethylbenzene	199, 200
Hydrogenation of CO_2	201
Fischer–Tropsch synthesis	202, 203
Selective oxidation of H_2S	204
Selective catalytic reduction of NO_x with hydrocarbons or NH_3	205, 206
Oxidation of alkanes with peroxides	207
Direct conversion of CH_4 to aromatics	208, 209

Table XII. Catalysis by Supported Cobalt Oxides

Catalytic reaction	Reference
Selective catalytic reduction of NO_x with hydrocarbons	210
Hydrodesulfurization of thiophene	211
Dehydrogenation of 1-butene	212
Total oxidation of hydrocarbons	213
Synthesis of higher alcohols	214
Fischer–Tropsch synthesis	215
Dehydration of methanol	216
Oxidation of saturated hydrocarbons with O_2	217
Oxidation of alkenes with O_2	218
Cracking of light alkanes	219
Autoxidation of cyclohexane	220

Table XIII. Catalysis by Supported Nickel Oxides

Catalytic reaction	Referenc
Dimerization of ethylene and propene	221
Cyclomerization of acetylene	221
Isomerization of *m*-xylene	222
Disproportionation of toluene	222
Hydrogenation of alkenes	223, 22
Hydrodesulfurization	223, 22
Oxidative dehydrogenation of isobutane	225
Oligomerization of propene	226
Transformation of isobutene into metacrylonitrile with NO	227

Table XIV. Catalysis by Supported Copper Oxides

Catalytic reaction	Reference
Direct decomposition of NO to N_2 and O_2	228
Selective oxidation of organic molecules with peroxides	229
Desulfurization of flue gas	230
Oxidation of CO	231
Combustion of CH_4	232
Selective catalytic reduction of NO_x with NH_3	233
Combustion of toluene	234
Hydrogenation of cyclopentadiene	235
Oxidation of phenol with oxygen or air	236
Complete oxidation of ethanol, acetaldehyde, and ethanol/methanol mixtures	237
Synthesis of methanol	238

Table XV. Catalysis by Supported Molybdenum Oxides

Catalytic reaction	Reference
Selective oxidation of methanol and ethanol	239–242
Hydrogenation of coal to crude oil	243
Metathesis of alkenes	244, 245
Direct conversion of CH_4 to aromatics	246–248
Selective catalytic reduction of NO_x with NH_3	249
Selective oxidation of propane with oxygen	250
Hydrodesulfurization	251–253
Hydrodemetallation	251–253
Hydrodenitrogenation	251–253
Isomerization of 1-butene	254
Oxidative dehydrogenation of propane	255
Reforming of alkanes and alkenes	256
Oxidation of ethanol with O_3	257
Partial oxidation of CH_4 and ethane	258, 259
Ammoxidation of ethylene	260, 261
Oxidation of propene	262
Epoxidation of fatty acid methylesters with peroxides	263
Polymerization of ethylene	264

both the gas phase and the liquid phase and are active in, for example, hydrogenation, dehydrogenation, dehydroaromatization, isomerization, selective oxidation, and selective reduction reactions. It is also clear that the same catalytic reaction can be catalyzed by different supported metal oxides, and, depending on the experimental conditions, one can turn a catalyst for a specific application into a system with totally different catalytic properties.

In what follows, we will discuss four selected examples of supported metal oxide catalysts. It will be shown that the detailed characterization of these catalysts allows us to develop structure–activity relationships and to obtain insight into the reaction mechanism of the catalytic process.

Table XVI. Catalysis by Supported Tungsten Oxides

Catalytic reaction	Reference
Hydroxylation of alkenes with peroxides	265, 266
Metathesis of alkenes	267
Partial oxidation of methane to formaldehyde	268
Isomerization of alkenes	269
Direct conversion of CH_4 to aromatics	270
Selective catalytic reduction of NO_x with NH_3	271
Homologation of alkenes	272
Hydrocarbon synthesis from methanol	273
Hydrodesulfurization	274
Hydrodenitrogenation	274
Isomerization of alkanes	275
Oxidative coupling of CH_4	276
Disproportionation and cyclotrimerization of alkynes	277
Homologation of ethene	278

Table XVII. Catalysis by Supported Rhenium Oxides

Catalytic reaction	Reference
Olefin metathesis	279
Selective catalytic reduction of NO_x with NH_3	280
Reactions of ethyldiazoacetate	281
Selective oxidation of organic molecules with peroxides	281
Selective oxidation of methanol	282
Hydrogenation of alkenes	283
Disproportionation of ethylene	284

Table XVIII. Catalysis by Supported Niobium Oxides

Catalytic reaction	Reference
Conversion of hydrocarbons	285
Selective oxidation of organic compounds	286
Isomerization of 1-butene	287
Hydrogenation of alkenes	288
Dehydrogenation of alkanes	289
Selective oxidation of methanol	290, 291
Selective catalytic reduction of NO_x with NH_3	292
Dehydrogenation of ethanol	293
Selective oxidation of ethanol	294
Aldol condensation of *n*-butyraldehyde	295

5.2. Selected Examples

5.2.1. Direct Conversion of Methane to Aromatics over Transition-Metal-Oxide-Supported H-ZSM-5 Catalysts

The catalytic conversion of methane to desired commodity chemicals is a challenging approach to the utilization of natural gas resources, and, consequently, considerable effort has been devoted to the development of novel catalytic systems. Oxygen has generally been used to activate methane, at the expense of losing some of the feedstock as carbon dioxide. The most extensively studied processes are the oxidative coupling of methane [296], partial oxidation of methane to synthesis gas [297], and the formation of oxygenated compounds such as methanol [298].

Several studies have also demonstrated that methane can be selectively converted to aromatics, such as benzene, toluene, and naphthalene, in the absence of an oxidant, for example, molecular oxygen [299–314]. This reaction can be written as

$$6CH_4 \rightarrow C_6H_6 + 9H_2 \quad (6)$$

Bragin et al. were the first to carry out the aromatization reaction of methane to benzene in a pulse reactor over a Pt-CrO_3/H-ZSM-5 catalyst at 750°C, and a methane conversion of 18% with 80% selectivity to benzene was obtained [299, 300]. Since then, mainly MoO_3/H-ZSM-5 catalysts have been studied in flow reactors at reaction temperatures of 700–800°C by several groups around the world, and a benzene selectivity of 70% was reached at a methane conversion of about 8%. XPS and reactivity studies have demonstrated that a metal carbide phase, namely Mo_2C, is the active phase in this methane activation process [308–314]. However, (sub)oxides of transition metal ions can also activate methane in the absence of oxygen, and the primary product, ethylene, undergoes subsequent oligomerization and cyclization reactions on Brönsted acid sites to form the aromatic products [20, 141, 142, 315].

Table XIX gives an overview of the catalytic properties of 2 wt% MeO_x/H-ZSM-5 catalysts for the reaction of methane at 750°C in the absence of oxygen [315]. This table summarizes the maximum methane conversion and the maximum selectivity toward benzene and aliphatic hydrocarbons (mainly C_2–C_3 hydrocarbons) as a function of the metal ion (Fe, V, W, and Cr), the preparation method (impregnation vs. solid-state ion exchange), and the pretreatment method (with or without CO prereduction at 500°C). It is clear from this table that the catalytic activity is strongly dependent on the identity of the transition metal ion and the pretreatment of the material. Optimum catalytic performances were obtained for MeO_x/H-ZSM-5 catalysts prereduced with CO. The maximum methane conversion decreased in the order Fe (4.1 %) > V (3.2 %) > W (2.4 %) > Cr (1.1 %). During an initial activation period, virtually no hydrocarbon products were formed and the major gas-phase products were CO, CO_2, and H_2O. The amount of CO and CO_2, gradually decreased with increasing time on stream and was almost totally absent after 4 h of reaction. Following this initial activation period, a benzene selectivity up to 70% was achieved. In addition, some naphthalene and toluene were formed, and a maximum selectivity toward aromatic hydrocarbons of more than 85% was reached after 4–6 h on stream. On the other hand, the selectivity toward C_2–C_3 hydrocarbons (mainly ethylene) increased continuously with increasing reaction time, as coke deposition gradually deactivated the acidic sites in the zeolite, where the ethylene undergoes secondary reaction. The formation of coke was confirmed by evaluating the carbon mass balance during methane activation and by measuring XPS spectra in the C1s region of active and deactivated catalysts.

Table XIX. Survey of the Catalytic and Spectroscopic Properties of 2.0 wt% TMI/H-ZSM-5 Catalysts for the Direct Conversion of Methane to Aromatics at 750°C in the Absence of Oxygen [315]

TMI[a]	Preparation method[b]	CO[c]	Maximum methane conversion (%)[d]	Selectivity toward benzene (%)	Selectivity toward C_2–C_3 (%)
Fe	SOL	No	0.8	0	17.7
		Yes	3.9	45.5	31.7
	IMP	No	4.1	61.8	19.4
		Yes	4.1	73.4	22.1
V	SOL	No	0.6	35.4	20.1
		Yes	0.6	35.5	19.1
	IMP	No	0.6	63.1	19.8
		Yes	3.2	31.6	20.4
W	SOL	No	0.3	0	12.7
		Yes	2.3	40.6	18.5
	IMP	No	0.7	0	16.9
		Yes	2.4	50.8	20.1
Cr	SOL	No	0.2	0	20.1
		Yes	0.5	28.2	64.9
	IMP	No	0.3	19.4	58.6
		Yes	1.1	72.0	26.7

[a] TMI, Transition metal ion.
[b] SOL, catalyst prepared via the solid-state ion-exchange procedure. IMP, catalyst prepared via the impregnation procedure.
[c] CO-treatment at 500°C for 6 h.
[d] As measured after 3 h of reaction.

The observed induction period decreases with increasing prereduction time with CO at moderate temperatures and with increasing metal ion loading. During this period, transition metal suboxides, namely V_2O_3, Cr_2O_3, Fe_3O_4, and WO_2, were formed, as was evidenced by XPS measurements. These XPS measurements were conducted on active catalyst samples, which immediately after quenching were transferred with an *in situ* device to the vacuum chamber of the XPS instrument. The initial activation of methane occurs on these reduced phases, leading to the formation of ethylene as the primary product. For samples prepared by impregnation, these reduced oxides were mainly located at the outer surface, and only a small fraction diffuses into the channels of the zeolite material. Only in the case of solid–state ion-exchanged samples did the transition metal ion react with the Brönsted acid sites during the preparation step. As a consequence, the differences in catalytic activity/selectivity between impregnated and solid-state ion-exchanged materials can be explained in terms of differences in zeolite acidity and the state of the transition metal oxide. In the case of solid-state ion-exchanged materials, the transition metal oxides are predominantly located in the zeolite channels at ion exchange sites. For catalysts prepared by impregnation, the transition metal oxides were preferentially anchored to the outer surface, probably as small clusters or a thin film of the reduced oxide, and only a small fraction diffused into the zeolite channels, where they replaced the protons at Brönsted acid sites.

The effect of the number of Brönsted acid sites on the activation of methane can be further evaluated by comparing MeO_x/H-ZSM-5 catalysts differing in their $Na^+ : H^+$ ratio and consequently in their number of Brönsted acid sites. It was observed that the methane conversion and benzene selectivity were close to zero for a catalyst material with no Brönsted acid sites. Furthermore, an increasing number of Brönsted hydroxyl groups resulted in a gradual increase in the conversion of methane and the formation of benzene. This result, together with the observation that pure ethylene can also be converted to aromatics over MeO_x/H-ZSM-5 catalysts, confirms the crucial role of acid sites in methane activation. The Brönsted acid sites are responsible for the oligomerization and conversion of the initially formed ethylene into benzene, toluene, and naphthalene. By doing so, the Brönsted acid sites shift the thermodynamically unfavorable equilibrium for the formation of ethylene to a more favorable equilibrium for the formation of aromatics. A possible reaction scheme of methane activation over MeO_x/H-ZSM-5 catalysts is given in Figure 23, showing the importance of the two active sites in the consecutive formation of ethylene and aromatics starting from methane [315]. In addition, two side reactions are indicated, namely the formation of coke on the reduced transition metal oxides dispersed on the H-ZSM-5 support and the back cracking of higher hydrocarbons.

It is also important to mention that catalytically inactive materials, such as Fe_3O_4/H-ZSM-5 catalysts, can be prepared via the solid-state ion-exchange method (Table XIX). This sample could be made active by a pretreatment with CO at 500°C for 6 h. During this pretreatment step, the outer surface of the zeolite material became enriched in supported iron oxides, as evidenced by XPS measurements. The resulting materials were much more active in methane conversion that the untreated samples. This illustrates the importance of

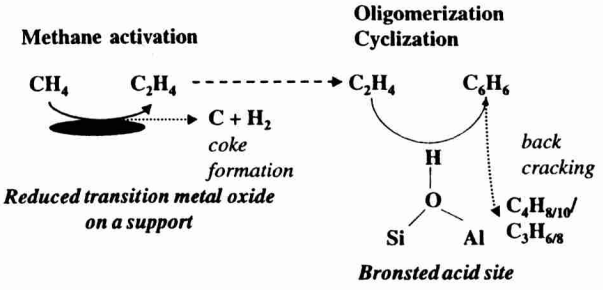

Fig. 23. Reaction scheme for the direct conversion of methane to aromatics over MeO_x/H-ZSM-5 catalysts. This process comprises two consecutive steps: the activation of methane over a reduced supported metal oxide and the oligomerization and cyclization of ethylene to aromatic compounds, such as benzene over a Brönsted acid site of the zeolite. Two side reactions can take place, namely the formation of coke at the surface of the supported metal oxide and the back cracking of higher hydrocarbons formed.

catalyst activation treatments on the dispersion of the transition metal oxides on the support surface and also underlines the critical interaction taking place at the metal oxide-support interface.

5.2.2. *Ethylene Polymerization over Cr-MCM-41 Catalysts*

In the early 1990s, Kresge et al. at Mobil reported the preparation of a new class of silica- and silica-alumina-based molecular sieves through the use of surfactant template molecules [316, 317]. The so-called mesoporous crystalline materials or M41S materials possess a periodic framework of regular mesopores, the size of which depends on the alkyl chain length of the template molecule used for the synthesis of this material. Mesoporous crystalline material (MCM)-41 is the most prominent example of the M41S family, and this material can be envisaged as a hexagonal tubular material with a very high surface area and with sharply defined pore diameters in the range of 2–10 nm. The discovery of these materials has greatly expanded the range of potential supports for the preparation of supported metal oxide catalysts.

Active transition metal oxide species can be grafted onto the inner surface of the mesopores of the MCM-41 material, which results in a material where all of the catalytically active sites are in principle accessible for reactant molecules. This has been shown to be possible for Ti [318] and Mn [319, 320], for example. Recently, it has been shown that well-defined chromium acetylacetonate complexes ($Cr(acac)_3$) can be grafted onto the surface of MCM-41 with the MDD method, giving rise to materials active in the polymerization of ethylene [321, 322]:

$$n CH_2CH_2 \rightarrow -(CH_2CH_2)_n- \qquad (7)$$

This catalytic reaction has been conducted in the gas phase at 100°C at 2.2 bar in a reactor vessel. The polymerization activity of several Cr-MCM-41 materials as a function of the support composition (with or without aluminium: AlMCM-41 and SiMCM-41 supports), the initial calcination temperaure (550 vs. 720°C), and the Cr loading (0–2 wt% Cr) are given in Table XX. It can be seen that

1. The pure SiMCM-41 and AlMCM-41 supports have some activity in the polymerization of ethylene.
2. The Cr-AlMCM-41 materials are more active than the Cr-SiMCM-41 materials;
3. The catalytic activity increases with increasing Cr loading up to 1 wt% Cr; higher Cr loadings result in less active Cr-MCM-41 materials.
4. The catalytic activity increases with increasing initial calcination temperature.

The latter observation can be explained by the presence of support hydroxyl groups, which are removed at higher calcination temperature. The catalytic activity passes through a maximum with increasing dehydroxylation, and an important factor influencing the degree of support dehydroxylation is the Cr loading. Since Cr and surface hydroxyl groups react during the catalyst activation with an anchoring mechanism, increasing Cr content increases dehydroxylation and thus catalyst activity. The decrease in polymerization activity above 1 wt% Cr loading must be due to the formation of Cr_2O_3 clusters on the MCM-41 surface, which are indeed observed with combined DRS-ESR spectroscopies.

Similar catalytic experiments can be performed in a reactor for slurry phase ethylene polymerization at 104°C. The catalytic performances, together with the characteristics of the polyethylene formed, are given in Table XXI for two catalysts with 1 wt% Cr [323]. It is clear that the Cr-AlMCM-41 catalyst is more than twice as active as the Cr-SiMCM-41 catalyst. The polymerization rate is about 140 g polyethylene/g catalyst/h, which is equivalent to 14,000 g polyethylene/g Cr/h. These values are much better than those obtained for Cr-Y zeolites. This difference must be due to the fact that the formation of polyethylene chains in the zeolite channels/pores is limited and that the chains block the active Cr sites after short polymerization runs. Because the zeolite materials do not readily break up during polymerization, low activities are usually observed. The Cr-MCM-41 catalysts break up during ethylene polymerization, and as a consequence these materials display a substantial and long-standing polymerization activity.

The melt index of a polymerization catalyst is as important as its catalytic activity. The melt index is a measure of the amount of molten polymer that can flow through a standard orifice under a set pressure in 10 minutes. The plastics formed with the Cr-MCM-41 catalysts have high load melt flow indices (HLMI) of 0.56 and 1.38 g/10 minutes for the Cr-AlMCM-41 and Cr-SiMCM-41 catalysts, respectively. These low numbers indicate a high molecular weight for the polyethylene formed (Table XX1) [323]. The origin of this difference between the two catalysts is unclear but may be caused by a different chemical composition of the support (Si : Al ratio of (∞ vs. 27) or a different pore diameter of the MCM-41 supports (28 vs. 25 Å) or a combination of both. Finally, the formation of polyethylene can be also confirmed by X-ray diffraction (XRD), differential scanning calorimetry

Table XX. Gas-Phase Polymerization of Ethylene over Cr-MCM-41 Catalysts: Effect of Support Composition, Calcination Temperature, and Cr Loading

Support	Cr loading (wt%)	Calcination temperature (°C)	Catalytic activity (g of polyethylene per g catalyst per hour)
Al-MCM-41	0.0	550	7.80
	0.5	550	15.36
	0.75	550	25.62
	1.0	550	26.10
	1.5	550	7.44
	2.0	550	10.74
	1.0	720	31.60
Si-MCM-41	0.0	550	6.00
	1.0	550	13.00

The catalytic activity is determined from the amount of ethylene consumed during the whole ethylene polymerization run of 2 h at 100°C and an initial ethylene pressure of 2.2 bar [322].

Table XXI. Slurry-Phase Polymerization of Ethylene over Cr-MCM-41 Catalysts Prepared by Grafting 1 wt% $Cr(acac)_3$ Complexes According to the MDD Method onto an Al-MCM-41 or SiMCM-41 Support

Catalyst	Catalytic activity (g polyethylene/g of Cr/h)	Polymer characteristics			
		MI5 (g/10 min)	HLMI (g/10 min)	SR5	Bulk density ($kg \cdot l^{-1}$)
Cr-AlMCM-41	14000	0.004	0.56	141	0.21
Cr-SiMCM-41	6300	0.028	1.38	49	0.20

The catalytic activity is determined from the amount of polyethylene formed during the whole ethylene polymerization run at an ethylene pressure of 31.4 bar and a reaction temperature of 104°C [256].

(DSC), and Fourier transform infrared spectroscopy (FTIR). XRD indicates the presence of crystalline polyethylene and some amorphous polyethylene. Thermal analysis of the polymer by DSC showed a single endotherm at 136°C, and FTIR indicated the characteristic vibrations of polyethylene.

One can also monitor the polymerizing Cr-MCM-41 with spectroscopic and microscopic techniques. To conduct spectroscopic measurements, a specially designed quartz cell equipped with an ESR tube and a DRS quartz window can be constructed that can withstand the polymerization conditions [323]. Combined DRS-ESR spectroscopies make it possible to evaluate at regular time intervals the oxidation state and coordination environment of Cr in the polymerizing Cr-MCM-41 catalyst. It was found that mainly Cr^{3+} species and some Cr^{2+} species are formed during the initial reaction steps by reduction of $Cr^{6+/5+}$ with ethylene. In addition, the near-infrared region of the DRS spectra shows the formation of overtone and combination bonds of the polyethylene formed during catalysis. It reconfirms the instant formation of polyethylene in the pores of the MCM-41 material. The catalyst particles gradually fragment, giving rise to a continuous distribution of the Cr-MCM-41 material in the polyethylene formed. This fragmentation process can be evaluated with scanning electron microscopy (SEM). SEM images of the catalyst, which was poisoned after 15 minutes of polymerization with CO, indicates that the outer surfaces of the wormlike Cr-MCM-41 particles are partially covered by fibers of polyethylene and that some of these catalyst particles break up. The bundles of polyethylene are 50–100 nm thick and have a length of 1 μm or more. These results show that the polymer chains are initially formed within the mesopores of the Cr-MCM-41 material, forming nanofibers of polyethylene with a length of several microns. Parts of these nanofibers protrude from the catalyst particle, while most of them (partially) cover the outer surface of the catalyst support. These catalyst particles further fragment during ethylene polymerization.

5.2.3. *Dehydrogenation of Alkanes over Supported Chromium Oxide Catalysts*

The catalytic dehydrogenation of alkanes has a very important industrial impact, because it represents an economical route to obtaining alkenes from feedstocks of low-cost saturated hydrocarbons [17, 323]. The dehydrogenation reactions of propane and isobutane are currently the most important. Propene is used for the synthesis of polypropylene in the polymer industry, and isobutene is used for the production of methyl t-butyl ether (MTBE) and ethyl t-butyl ether (ETBE). MTBE and ETBE are additives to gasoline, but their use is currently under debate, especially in the United States. Its phase-out could have an influence on the production plants for isobutene. Most probably, these chemical plants will have to change to the dehydrogenation of propane, because it is anticipated that the demand for propene will increase in the next decades.

One of the most important goals of current catalyst research is to develop quantitative structure–activity relationships and

to elucidate the nature of the active site of a heterogeneous catalyst. This has recently been done for the dehydrogenation of isobutane of alkanes over supported chromium oxide catalysts [324]. The approach is based on the use of experimental design. This is a technique that has been successfully introduced in the field of drug and pharmaceuticals design in the past, but until recently, to our best knowledge, not in the field of heterogeneous catalysis. The spectroscopic technique used is *in situ* DRS spectroscopy, which allows monitoring of the amount of Cr^{6+}, Cr^{3+}, and Cr^{2+} in the catalyst material during isobutane dehydrogenation.

The developed method involves a four-pronged approach. In a first step, the number of required experiments has been optimized by the use of an experimental design, and five experimental parameters or factors were selected to describe the dehydrogenation process: (a) the $SiO_2 : Al_2O_3$ ratio of the silica-alumina support used in this study (this difference in chemical composition is expressed by the IEP of the support and is denoted as X_1), (b) the Cr loading (X_2), (c) the gas composition (i.e., the percentage of isobutane in a N_2 stream (X_3)), (d) the reaction temperature (X_4), and (e) the reaction time (X_5). A five-level circumscribed central composite experimental design resulted in a set of 30 experiments. The experimental conditions for these 30 measurements are summarized in Table XXII.

Second, the dehydrogenation activity was measured by on-line GC analysis for the set of 30 experiments. The catalyst activities, indicated by the response values y, are summarized in Table XXII. The selectivities toward isobutene were always very high and reached a maximum at around 90–95%. This indicates that the catalytic conversions in the *in situ* DRS cell are a good measure of the catalytic performances of the supported chromium oxide catalysts. The influence of the different design variables or factors on the response value y can be determined by applying a statistical model based on multiple linear regression. This analysis resulted in the following quantitative relationship:

$$\begin{aligned} y^{1/2}(\%) = {} & 2.284 - 0.195 \times X_1 + 0.121 \times X_2 - 0.132 \times X_3 \\ & - 9.540 \times 10^{-4} \times X_4 - 0.0610 \times X_5 \\ & + 4.941 \times 10^{-3} \times X_3^2 + 5.875 \times 10^{-4} \times X_5^2 \\ & + 5.137 \times 10^{-4} \times X_1 \times X_4 - 4.480 \times 10^{-3} \\ & \times X_2 \times X_3 + 8.008 \times 10^{-4} \times X_3 \times X_5 \end{aligned} \quad (8)$$

This equation allows the calculation of the conditions for maximum dehydrogenation activity over supported chromium oxide catalysts. The following conditions were obtained: $X_1 = 8$, $X_2 = 7.5$, $X_3 = 2$, $X_4 = 500$, and $X_5 = 10$. Thus, a

Table XXII. Experimental Design for Optimizing the Isobutane Dehydrogenation over Supported Chromium Oxide Catalysts [324]

Experiment number	Experiment name	Run order	X_1	X_2	X_3	X_4	X_5	y	Z
1	N01	12	2	0.5	2	350	50	0.070	0.090
2	N02	26	8	0.5	2	350	10	0.63	0.17
3	N03	8	2	7.5	2	350	10	4.30	1.26
4	N04	9	8	7.5	2	350	50	0.88	2.55
5	N05	4	2	0.5	18	350	10	0.44	0.086
6	N06	27	8	0.5	18	350	50	0.090	0.23
7	N07	18	2	7.5	18	350	50	0.33	1.29
8	N08	2	8	7.5	18	350	10	1.26	2.52
9	N09	13	2	0.5	2	500	10	1.71	0.24
10	N10	10	8	0.5	2	500	50	0.24	0.65
11	N11	19	2	7.5	2	500	50	1.18	3.57
12	N12	21	8	7.5	2	500	10	5.18	7.23
13	N13	17	2	0.5	18	500	50	0.090	0.25
14	N14	5	8	0.5	18	500	10	1.40	0.65
15	N15	3	2	7.5	18	500	10	1.09	3.66
16	N16	11	8	7.5	18	500	50	1.48	7.15
17	N17	6	2	4	10	425	30	0.040	0.78
18	N18	1	8	4	10	425	30	0.20	2.35
19	N19	23	5	0.1	10	425	30	0.05	0.080
20	N20	22	5	8	10	425	30	0.11	0.54
21	N21	24	5	4	1	425	30	1.77	1.16
22	N22	14	5	4	19	425	30	0.090	1.25
23	N23	7	5	4	10	300	30	0.12	0.65
24	N24	15	5	4	10	550	30	0.73	5.80
25	N25	20	5	4	10	425	5	1.75	1.10
26	N26	16	5	4	10	425	55	0.060	1.25
27	N27	25	5	4	10	425	30	0.090	1.26
28	N28	28	5	4	10	425	30	0.090	1.25
29	N29	29	5	4	10	350	30	0.24	0.48
30	N30	30	5	0.55	10	350	30	0.070	0.13

maximum conversion is obtained after 10 minutes for a 7.5 wt% CrO_3/Al_2O_3 catalyst at 500°C with a mixture of 2% isobutane in N_2. The conversions are still, however, relatively low because of the experimental limitations of the *in situ* DRS cell. Thus, an optimal dehydrogenation activity is expected for a high-loaded CrO_3/Al_2O_3 catalyst working in the temperature range of 550–625°C and at shorter reaction times.

In a third step, the Cr speciation was measured by *in situ* DRS spectroscopy with the use of a special *in situ* reaction chamber. An example of a set of *in situ* DRS spectra is given in Figure 24. This is an experiment with a 0.5 wt% CrO_3/SiO_2 catalyst treated at 350°C in a 2% isobutane stream. Figure 24 shows a gradual decrease in the absorption maxima around 360 nm and 450 nm with increasing reaction time at the expense of a new weak band with an absorption maximum at around 625 nm. The inset of Figure 24 illustrates the presence of an isobestic point, suggesting the presence of two different Cr species. By applying statistical routines for spectral analysis to the set of DRS spectra, two pure component spectra were revealed. The two pure component spectra have absorption maxima at around 360 nm and 625 nm. The first pure component is indicative of the presence of Cr^{6+}, whereas the second pure component spectrum is typical for the presence of $Cr^{2+/3+}$. It has been shown that the band intensity of the $Cr^{2+/3+}$ species increases with increasing reaction temperature and with the IEP of the support. The band intensities are denoted as the response values z and are summarized for each of the catalysts in Table XXII.

In a fourth and final step, a mathematical relation that relates the dehydrogenation activity with the amount of *in situ* measured $Cr^{3+/2+}$ was derived. This is illustrated in Figure 25 for CrO_3/Al_2O_3 catalysts. It can be concluded that the catalytic activity (response y) is directly proportional to the amount of the reduced Cr species (response z). The difference in catalytic activity between the CrO_3/Al_2O_3 catalysts, which were 10 or 50 minutes on stream, must be explained in terms of coking. The higher the amount of coke at the catalyst surface, the lower the catalyst activity. This coke is removed in an industrial reactor by a calcination treatment. Finally, it is important to stress that this analysis does not discriminate between Cr^{2+} and Cr^{3+} and does not unambiguously assign the catalytic

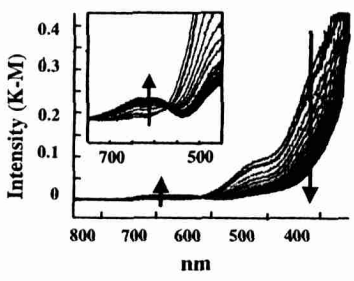

Fig. 24. *In situ* DRS spectra of a 0.5 wt% CrO_3/SiO_2 catalyst during isobutane dehydrogenation at 350°C in a 2% isobutane stream as a function of time on stream. The inset illustrates the presence of an isobestic point, which is indicative of the presence of two different Cr species. (Copyright 1999 Elsevier Science BV.)

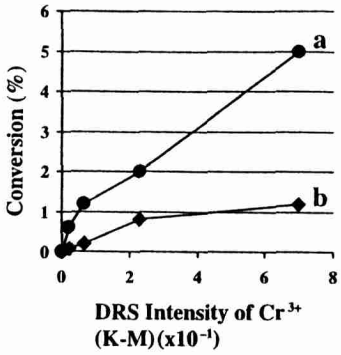

Fig. 25. Quantitative relationship between the catalytic activity in the dehydrogenation of isobutane over supported CrO_3/Al_2O_3 catalysts (as expressed by the response y) and the amount of reduced Cr species (as expressed by the response z), as predicted for 10 (a) and 50 (b) minutes on stream.

activity to one of these species. In any case, there are indications that Cr^{2+} is less active than Cr^{3+} for alkane dehydrogenation because the relative amount of Cr^{3+} species increases with increasing Al_2O_3 content of $SiO_2 \cdot Al_2O_3$ supports, and the catalytic activity also increases with increasing Al_2O_3 content of the supports [325]. The nature of these Cr^{3+} species has been further unraveled by infrared spectroscopy with CO and NO as probe molecules. De Rossi et al. have shown that isolated Cr^{3+} sites with two coordinative vacancies are formed in CrO_3/Al_2O_3 catalysts during alkane dehydrogenation [326], and it is anticipated that these centers are responsible for the activation of the alkane molecules in the absence of oxygen.

5.2.4. *NO Decomposition over Cu/ZSM-5 Catalysts*

Most fossil fuels have small amounts of nitrogen-containing compounds, which will yield emissions of nitrogen oxides, commonly denoted as NO_x, although they consist mainly of NO and small amounts of N_2O. According to thermodynamics, NO is an unstable molecule even at very high temperatures. However, the decomposition rate of the reaction

$$2NO \rightarrow N_2 + O_2 \qquad (9)$$

is very low, and hence it is necessary to use an appropriate heterogeneous catalyst for this decomposition reaction. Many studies have been devoted to the development of such catalysts, and interesting examples are Pt on alumina, perovskites, supported metal oxides, and unsupported metal oxides, such as Co_2O_4, CuO, NiO, Fe_2O_3, and ZrO_2 [327–329]. The most important discovery in this field has been made by the group of Iwamoto in Japan in 1986 [330]. They observed that Cu/ZSM-5 zeolites have a very high activity in the catalytic decomposition of NO at relatively low temperatures.

Iwamoto et al. showed in further studies that the catalytic activity increases between 300°C and 450°C to reach a maximum activity between 450°C and 500°C [331, 332]. The catalytic activity decreases again at higher temperatures. Important here is the desorption process of O_2 molecules from

the catalyst surface, because it is observed that this molecule inhibits the decomposition reaction. At temperatures above 300°C, O_2 molecules readily desorb from the catalyst surface and the catalyst becomes active. Furthermore, the exchange level of Cu^{2+} has an influence on the catalytic conversion, and exchange levels above 100% are necessary to obtain very high activities.

Valyon and Hall used isotopically labeled molecules, such as $^{18}O_2$ and $^{15}N^{18}O$, to study the release of O_2 during the decomposition reaction [333]. It was shown that during the decomposition of NO the oxygen atom of the NO molecule is attached to the surface of the ZSM-5 zeolite. Molecular oxygen leaves the surface and consists of the chemisorbed oxygen and lattice oxygen. In addition, the presence of a nitrogen dioxide surface species was detected at the catalyst surface.

Iwamoto et al. have investigated the reaction mechanism of the NO decomposition over Cu-ZSM-5 zeolites in rather great detail via IR spectroscopy in combination with isotopic tracer studies [330–332, 334, 335]. A mixture of NO and He was passed over the catalytic bed at room temperature, and N_2 was released from the catalyst surface after 12 minutes on stream. The amount of N_2 formed went through a maximum and dropped to zero after 60 minutes on stream. After 45 minutes N_2O started to evolve, and a maximum amount of this component was observed after 100 minutes on stream, and then it gradually decreased. After 350 minutes no reactions occurred in the catalyst bed. The catalytic reaction can be initiated by heating the material up to 300°C, and the active sites (i.e., Cu^+) are regenerated by desorption of O_2 molecules. The three surface species $(NO)_2^{\delta-}$, $NO^{\delta+}$ and $NO^{\delta-}$ were detected by IR spectroscopy. $NO^{\delta+}$ is formed on Cu^{2+} sites, and the electron of the $2p\pi*$ orbital of NO is partially given to Cu^{2+}, whereas the $NO^{\delta-}$ species is formed on Cu^+ sites. The latter Cu^+ species will give partially an electron from its d-orbital to the $2p\pi^*$ orbital of NO. It was observed that the amount of the $NO^{\delta-}$ species decreases with time, whereas the amount of the $NO^{\delta+}$ species at the surface increases.

On the basis of their spectroscopic results, Iwamoto et al. have proposed a reaction mechanism, which is shown in Figure 26 [330]. Because of the heating of the catalyst, Cu^{2+} is partially reduced to Cu^+, which is the active site for the NO decomposition process. They are the adsorption sites for NO, and $(NO)_2^{\delta-}$ and $NO^{\delta-}$ (species I, II, III, and IV) are formed at the catalyst surface. These species can react with $(NO)_2^{\delta-}$ and $NO^{\delta+}$ species, which are adsorbed on neighboring Cu^+ sites (species VI and VII). This reaction results in the formation of N_2 or N_2O. One oxygen atom remains at the surface and oxidizes Cu^+ to Cu^{2+} (species V). These Cu^{2+} species can again adsorb NO as $NO^{\delta+}$ (species VI and VII). It is important in this model that it involves the interaction between two neighboring Cu sites.

Another mechanism was proposed by Schneider et al. [336]. This group has used theoretical calculations based on density functional theory (DFT) to unravel the decomposition process over Cu-ZSM-5 catalysts. They have calculated for three different models (free Cu, Cu bounded in a twofold way to $Si(OH)_4$, and Cu bounded in a twofold way to $Al(OH)_4$) the energy of the possible reaction intermediates for the successive reaction between Cu^+ and two NO molecules. On this basis, they proposed the reaction scheme given in Figure 27. This reaction mechanism involves two main reaction steps. The first is the binding of two NO molecules zeolitic Cu^+ (ZCu) to form a dinitrosyl species, which is experimentally observed, for example, by Giamello et al. by vibrational spectroscopies [337]. There is also the release of N_2O molecules:

$$ZCu + 2NO \rightarrow [ZCuONNO] \rightarrow ZCuO + N_2O \qquad (10)$$

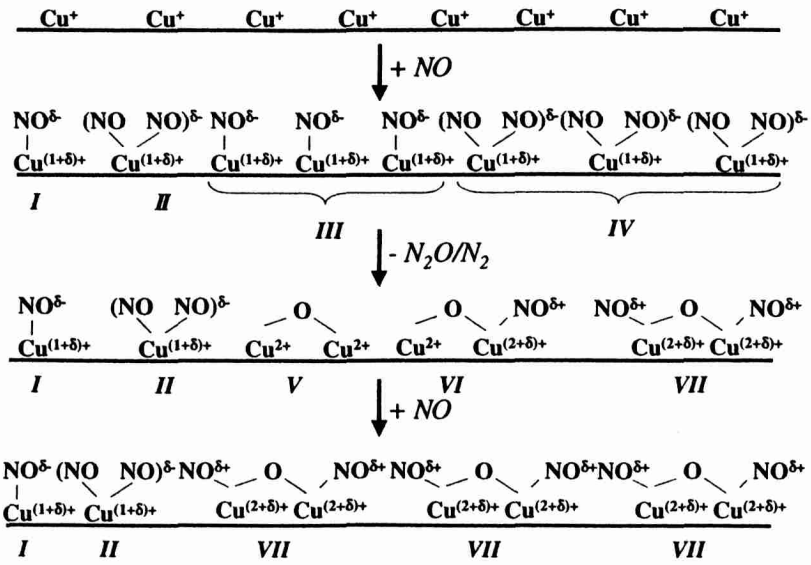

Fig. 26. Reaction mechanism for the direct decomposition of NO over Cu/ZSM-5 catalysts as proposed by Iwamoto et al. [331]. This mechanism is based mainly on IR measurements. (Copyright 1992 American Chemical Society.)

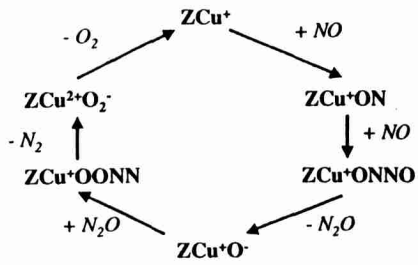

Fig. 27. Reaction mechanism for the direct decomposition of NO over Cu/ZSM-5 catalysts as proposed by Schneider et al. [336]. This mechanism is based on theoretical calculations, and some of the reaction steps are supported by experimental observations. (Copyright 1998 American Chemical Society.)

This reaction is exothermic. The gas-phase intermediate N_2O will readsorb in a second step to ZCuO with the formation of N_2 according to

$$ZCuO + N_2O \rightarrow [ZCuOONN] \rightarrow ZCuO_2 + N_2 \qquad (11)$$

This reaction is the rate-determining step. Schneider et al. also concluded that no two neighboring Cu^{2+} sites are necessary to explain the catalytic activity of Cu-ZSM-5 zeolites [336]. This is in contrast to the model of Iwamoto et al. [331]. This difference in opinion also suggests that further studies have to aim for a combined approach of theoretical calculations on relevant model systems and *in situ* time-resolved spectroscopic measurements.

ABBREVIATIONS

AEC	Anion exchange capacity
AES	Auger electron spectroscopy
AFM	Atomic force microscopy
ALE	Atomic layer epitaxy
CEC	Cation exchange capacity
CVD	Chemical vapor deposition
DFT	Density functional theory
DRS	Diffuse reflectance spectroscopy in the UV-Vis-NIR (ultraviolet visible near infrared region)
DSC	Differential scanning calorimetry
EELS	Electron energy loss spectroscopy
ESR	Electron spin resonance
EXAFS	Extended X-ray absorption fine structure
FCC	Fluid catalytic cracking
FEM	Field emission microscopy
FIM	Field ion microscopy
FTIR	Fourier transform infrared spectroscopy
HDPE	High-density polyethylene
HLMI	High load melt flow index
IEC	Ion exchange capacity
IEP	Isoelectric point
IR	Infrared spectroscopy
LDH	Layered double hydroxide
LEED	Low-energy electron diffraction
LEIS	Low-energy ion scattering
LLDPE	Linear low-density polyethylene
M	Metal ion
MCM	Mesoporous crystalline material
MDD	Molecularly designed dispersion
Me	Metal ion
MES	Mössbauer emission spectroscopy
NMR	Nuclear magnetic resonance
PZC	Point of zero charge
RBS	Rutherford backscattering
RS	Raman spectroscopy
S	Support
SEM	Scanning electron microscopy
SIMS	Secondary ion mass spectroscopy
SNMS	Secondary neutral mass spectroscopy
STM	Scanning tunneling microscopy
TDS	Thermal desorption spectroscopy
TEM	Transmission electron microscopy
TOF	Turnover frequency
TPD	Temperature-programmed desorption
TPO	Temperature-programmed oxidation
TPR	Temperature-programmed reduction
TPRS	Temperature-programmed reaction spectroscopy
UPS	Ultraviolet X-ray photoelectron spectroscopy
USY	Ultrastable Y zeolite
XANES	X-ray absorption near-edge structure
XAS	X-ray absorption spectroscopy
XPS	X-ray photoelectron spectroscopy
XRD	X-ray diffraction
Z	Zeolite

6. CONCLUDING REMARKS AND A LOOK INTO THE FUTURE

It has been shown that supported metal oxides are very complex inorganic materials that play a crucial role in heterogeneous catalysis in both the gas and liquid phase. Their synthesis and molecular design require a profound knowledge of both solid-state chemistry and inorganic chemistry, and their application as heterogeneous catalysts in various pharmaceutical, chemical, petrochemical, and environmental processes results from the specific interaction between the support and the metal oxides. Insight into the preparation of supported metal oxide catalysts at the molecular level would be very important to an understanding of the different steps involved. It is hoped that this goal can be achieved in the near future by the application of *in situ* spectroscopic techniques.

It is also evident from this review article that the support characteristics (i.e., structure and chemical composition) have a tremendous impact on the properties of the supported metal oxide species. This support effect results in the formation of specific, often unknown, molecular structures of metal oxides with, for example, special redox properties. A better insight into the formation and local structure of these molecular structures can only be obtained by applying a battery of complementary characterization techniques, preferably

ıder *in situ* conditions. Thus, a multitechnique approach is quired. The ultimate goal of such characterization studies to develop quantitative structure–activity relationships or to :velop expert systems for on line control of catalytic reactors. ıch information is still not available for most of the sup-ɔrted metal oxide catalyts currently available. Therefore, fur-er research has to be directed toward the reaction mechanism supported metal oxide catalysts at the molecular level. The-etical calculations of relevant cluster models of supported etal oxide catalysts can be helpful in this respect because ey can provide insight into the interpretation of spectro-opic data as well as the catalytic reaction mechanism.

cknowledgments

he financial support of the Fund of Scientific Research–landers (Belgium), the Concerted Research Action of the lemish Government (Belgium), the National Science Foun-ıtion (U.S.), and the Division of Basic Energy Sciences, epartment of Energy (U.S.), is greatly acknowledged. .M.W. was a research fellow of the Fund of Scientific esearch–Flanders (F.W.O.) at K. U. Leuven. This paper dedicated to the undergraduate, graduate, and postdoc-ıral students at K. U. Leuven (L. De Ridder, H. Spooren, . Verberckmoes, A. Buttiens, I. Vannijvel, B. Schoofs, . De Baets, M. Groothaert, S. Kijlstra, G. Catana, R. R. ao, A. Bensalem, and X. Gao) and Lehigh University . D. Hardcastle, J. M. Jehng, G. Deo, M. A. Vuurman, D. S. im, M. A. Banares, H. Hu, Y. Cai, X. Gao, and C. B. Wang) ho have made significant contributions to this field over the ıst decade.

EFERENCES

1. G. Ertl, H. Knozinger, and J. Weitkamp (Eds.), "Handbook of Heterogeneous Catalysis," Wiley–VCH, Weinheim, 1997.
2. B. M. Weckhuysen, P. Van Der Voort, and G. Catana (Eds.), "Spectroscopy of Transition Metal Ions on Surfaces," Leuven Univ. Press, Leuven, Belgium, 2000.
3. J. M. Thomas and W. J. Thomas, "Principles and Practice of Heterogeneous Catalysis," VCH, Weinheim, 1997.
4. F. Delannay (Ed.), "Characterization of Heterogeneous Catalysts," Dekker, New York/Basel, 1984.
5. W. N. Delgass, G. L. Haller, R. Kellerman, and J. H. Lunsford, "Spectroscopy in Heterogeneous Catalysis," Academic Press, New York, 1979.
6. R. L. Park, "Experimental Methods in Catalytic Research," Vol. 3 (R. B. Anderson and P. T. Dawson, Eds.), Academic Press, New York, 1976.
7. H. H. Kung, "Transition Metal Oxides, Surface Chemistry and Catalysis," Elsevier, Amsterdam, 1989.
8. I. E. Wachs (Ed.), "Characterization of Catalytic Materials," Butterworth–Heineman, New York, 1992.
9. J. W. Niemantsverdriet, "Spectroscopy in Catalysis, An Introduction," VCH, Weinheim, 1993.
10. J. Hagen, "Industrial Catalysis, A Practical Approach," Wiley-VCH, Weinheim, 1999.
11. G. Ertl, H. Knozinger, and J. Weitkamp (Eds.), "Environmental Catalysis," Wiley–VCH, Weinheim, 1999.
12. G. Ertl, H. Knozinger, and J. Weitkamp (Eds.), "Preparation of Solid Catalysts," Wiley–VCH, Weinheim, 1999.
13. R. A. van Santen, "Theoretical Heterogeneous Catalysis," World Scientific Lecture and Course Notes in Chemistry, Vol. 5, World Scientific, London, 1991.
14. B. M. Weckhuysen and R. A. Schoonheydt, *Rev. Roumaine Chim.* 44, 1047 (1999).
15. D. Sanfilippo (Ed.), "The Catalytic Process from Laboratory to the Industrial Plant," Italian Chemical Society, Rimini, 1994.
16. J. F. Le Page, "Applied Heterogeneous Catalysis—Design, Manufacture, Use of Solid Catalysts," Editions Technip, Paris, 1987.
17. B. M. Weckhuysen and R. A. Schoonheydt, *Catal. Today* 51, 223 (1999).
18. N. N. Greenwood and A. Earnshaw, "Chemistry of the Elements," Pergamon, Oxford, 1984.
19. B. M. Weckhuysen, I. E. Wachs, and R. A. Schoonheydt, *Chem. Rev.* 96, 3327 (1996).
20. B. M. Weckhuysen, D. Wang, M. P. Rosynek, and J. H. Lunsford, *Angew. Chem. Int. Ed. Engl.* 36, 2374 (1997).
21. B. M. Weckhuysen and R. A. Schoonheydt, *Catal. Today* 51, 215 (1999).
22. M. P. McDaniel, *Adv. Catal.* 33, 47 (1985).
23. D. E. De Vos, P. P. Knops-Gerrits, R. F. Parton, B. M. Weckhuysen, P. A. Jacobs, and R. A. Schoonheydt, *J. Inclus. Phen. Mol. Recogn. Chem.* 21, 185 (1995).
24. M. Che, *Stud. Surf. Sci. Catal.* 75A, 21 (1993).
25. J. T. Richardson, "Principles of Catalyst Development," Plenum, New York, 1989.
26. G. C. Bond and S. F. Tahir, *Appl. Catal.* 71, 1 (1991).
27. B. Sels, D. De Vos, M. Buntinx, F. Pierard, A. Kirsch-De Mesmaeker and P. Jacobs, *Nature (London)* 400, 855 (1999).
28. P. Van Der Voort, M. G. White, and E. F. Vansant, *Langmuir* 14, 106 (1998).
29. A. Kytokovi, J. P. Jacobs, A. Hakuli, J. Merilainen, and H. H. Brongersma, *J. Catal.* 162, 190 (1996).
30. S. Haukka, A. Kytokivi, E. L. Lakomaa, U. Lehtovirta, M. Lindblad, V. Lujala, and T. Suntola, *Stud. Surf. Sci. Catal.* 91, 957 (1995).
31. B. M. Weckhuysen, R. R. Rao, J. A. Martens, and R. A. Schoonheydt, *Eur. J. Inorg. Chem.* 565 (1999).
32. J. Haber, *J. Pure Appl. Chem.* 56, 1663 (1984).
33. Y. C. Xie and Y. Q. Tang, *Adv. Catal.* 31, 1 (1990).
34. H. Knozinger and E. Taglauer, *Catalysis* 10, 1 (1993).
35. J. C. Mol, *Catal. Today* 51, 289 (1999).
36. I. E. Wachs and B. M. Weckhuysen, *Appl. Catal. A General* 157, 67 (1997).
37. H. Bosch and F. Janssen, *Catal. Today* 2, 369 (1988).
38. G. Deo and I. E. Wachs, *J. Phys. Chem.* 95, 5889 (1991).
39. B. M. Weckhuysen, R. A. Schoonheydt, J. M. Jehng, I. E. Wachs, S. J. Cho, R. Ryoo, S. Kijlstra, and E. Poels, *J. Chem. Soc. Faraday Trans.* 91, 3245 (1991).
40. A. M. Turek, I. E. Wachs, and E. DeCanio, *J. Phys. Chem.* 96, 5000 (1992).
41. I. E. Wachs, Colloids and surfaces. A. *Physichem. Eng. Aspects* 105, 143 (1995).
42. B. M. Weckhuysen, J. M. Jehng, and I. E. Wachs, *J. Phys. Chem. B* 104, 7382 (2000).
43. B. M. Weckhuysen and I. E. Wachs, *J. Phys. Chem. B* 101, 2793 (1997).
44. M. A. Vuurman and I. E. Wachs, *J. Phys. Chem.* 96, 5008 (1992).
45. O. Saur, M. Bensitel, A. B. Mohammed Saad, J. C. Lavalley, C. P. Tripp, and B. A. Morrow, *J. Catal.* 99, 104 (1986).
46. B. M. Weckhuysen and I. E. Wachs, *J. Phys. Chem.* 100, 14437 (1996).
47. L. J. Burcham, G. Deo, X. Gao, and I. E. Wachs, *Top. Catal.* 11, 85 (2000).
48. F. D. Hardcastle and I. E. Wachs, *J. Phys. Chem.* 95, 5031 (1991).
49. X. Gao, S. R. Bare, B. M. Weckhuysen, and I. E. Wachs, *J. Phys. Chem. B* 102, 10842 (1998).

50. I. E. Wachs, *Top. Catal.* 8, 57 (1999).
51. B. M. Weckhuysen, L. M. De Ridder, and R. A. Schoonheydt, *J. Phys. Chem.* 97, 4756 (1993).
52. B. M. Weckhuysen, A. A. Verberckmoes, A. L. Buttiens, and R. A. Schoonheydt, *J. Phys. Chem.* 98, 579 (1994).
53. B. M. Weckhuysen, L. M. De Ridder, P. J. Grobet, and R. A. Schoonheydt, *J. Phys. Chem.* 99, 320 (1995).
54. B. M. Weckhuysen, H. J. Spooren, and R. A. Schoonheydt, *Zeolites* 14, 450 (1994).
55. G. Catana, R. R. Rao, B. M. Weckhuysen, P. Van Der Voort, E. Vansant, and R. A. Schoonheydt, *J. Phys. Chem. B* 102, 8005 (1998).
56. A. Bensalem, B. M. Weckhuysen, and R. A. Schoonheydt, *J. Phys. Chem. B* 101, 2824 (1997).
57. A. Bensalem, B. M. Weckhuysen, and R. A. Schoonheydt, *J. Chem. Soc. Faraday Trans.* 93, 4065 (1997).
58. M. A. Banares, J. H. Cardoso, F. Agullo-Rueda, J. M. Correa-Bueno, and J. L. G. Fierro, *Catal. Lett.* 64, 191 (2000).
59. B. M. Weckhuysen, I. E. Wachs, and R. A. Schoonheydt, *Stud. Surf. Sci. Catal.* 91, 151 (1995).
60. I. E. Wachs, G. Deo, M. V. Juskelis, and B. M. Weckhuysen, *Stud. Surf. Sci. Catal.* 109, 305 (1997).
61. I. E. Wachs, G. Deo, B. M. Weckhuysen, A. Andreini, M. A. Vuurman, M. De Boer, and M. D. Amiridis, *J. Catal.* 161, 211 (1996).
62. I. E. Wachs, J. M. Jehng, G. Deo, B. M. Weckhuysen, V. V. Guliants, and J. B. Benziger, *Catal. Today* 32, 47 (1996).
63. I. E. Wachs, J. M. Jehng, G. Deo, B. M. Weckhuysen, V. V. Guliants, J. B. Benziger, and S. Sundaresan, *J. Catal.* 170, 75 (1997).
64. C. B. Wang, Y. Cai, and I. E. Wachs, *Langmuir* 15, 1223 (1999).
65. Y. Cai, C. B. Wang, and I. E. Wachs, *Stud. Surf. Sci. Catal.* 110, 255 (1997).
66. M. Ruitenbeek, A. J. van Dillen, F. M. F. de Groot, I. E. Wachs, J. W. Geus, and D. C. Koningsberger, *Top. Catal.* 10, 241 (2000).
67. G. Dagan, S. Sampath, and O. Lev, *Chem. Mater.* 7, 446 (1995).
68. R. W. Matthews, *J. Catal.* 113, 549 (1998).
69. H. Inoue, T. Matsuyama, B. Liu, T. Sakata, H. Mori, and H. Yoneyama, *Chem. Lett.* 653 (1994).
70. M. Anpo and K. Chiba, *J. Mol. Catal.* 74, 207 (1992).
71. C. Anderson and A. J. Bard, *J. Phys. Chem.* 99, 9882 (1995).
72. C. Anderson and A. J. Bard, *J. Phys. Chem. B* 101, 2611 (1997).
73. X. Fu, L. A. Clark, Q. Yang, and M. A. Anderson, *Environ. Sci. Technol.* 30, 647 (1996).
74. S. Yoshida, S. Takenaka, T. Tanaka, H. Hirano, and H. Hayashi, *Stud. Surf. Sci. Catal.* 101, 871 (1996).
75. S. Imamura, H. Tarumoto, and S. Ishida, *Ind. Eng. Chem. Res.* 28, 1449 (1989).
76. S. Imamura, T. Higashihara, and H. Jindai, *Chem. Lett.* 1667 (1993).
77. T. Liu and T. Cheng, *Catal. Today* 26, 71 (1995).
78. Z. Liu, J. Tabora, and R. J. Davis, *J. Catal.* 149, 117 (1994).
79. A. Molnar, M. Bartok, M. Schneider, and A. Baiker, *Catal. Lett.* 43, 123 (1997).
80. P. K. Doolin, S. Alerasool, D. J. Zalewski, and J. F. Hoffman, *Catal. Lett.* 25, 209 (1994).
81. M. Itoh, H. Hattori, and K. Tanabe, *J. Catal.* 35, 225 (1974).
82. J. R. Sohn and J. H. Jang, *J. Catal.* 132, 563 (1991).
83. W. F. Maier, J. A. Martens, S. Klein, J. Heilmann, R. Parton, K. Vercruysse, and P. A. Jacobs, *Angew. Chem.* 108, 222 (1996).
84. S. Srinivasan, A. K. Datye, M. Hampden-Smith, I. E. Wachs, G. Deo, J. M. Jehng, A. M. Turek, and C. H. F. Peden, *J. Catal.* 131, 260 (1991).
85. C. B. Khouw, C. B. Dartt, J. A. Labinger, and M. E. Davis, *J. Catal.* 149, 195 (1994).
86. A. Bendandi, G. Fornasari, M. Guidoreni, L. Kubelkova, M. Lucarini, and F. Trifiro, *Top. Catal.* 3, 337 (1996).
87. R. Hutter, D. C. M. Dutoit, T. Mallat, M. Schneidez, and A. Baiker, *J. Chem. Soc. Chem. Commun.* 163 (1995).
88. R. Hutter, T. Mallat, and A. Baiker, *J. Catal.* 153, 665 (1995).
89. Z. Liu, G. M. Crumbaugh, and R. J. Davis, *J. Catal.* 159, 83 (1996).
90. R. Hutter, T. Mallat, and A. Baiker, *J. Catal.* 153, 177 (1995).
91. R. A. Sheldon and J. A. Van Doorn, *J. Catal.* 31, 427 (1973).
92. S. Klein, J. A. Martens, R. Parton, K. Vercruysse, P. A. Jacobs, and W. F. Maier, *Catal. Lett.* 38, 209 (1995).
93. A. Keshavaraja, V. Ramaswamy, H. S. Soni, A. V. Ramaszamy, and P. Ratnasamy, *J. Catal.* 157, 501 (1995).
94. D. R. C. Huybrechts, L. De Bruycker, and P. A. Jacobs, *Nature (London)* 345, 240 (1990).
95. S. Srinivasan, A. K. Datye, M. Hampden-Smith, I. E. Wachs, G. Deo, J. M. Jehng, A. M. Turek, and C. H. F. Peden, *J. Catal.* 131, 260 (1991).
96. G. Deo, A. M. Turek, I. E. Wachs, D. R. C. Huybrechts, and P. A. Jacobs, *Zeolites* 13, 656 (1994).
97. W. B. Kim and J. S. Lee, *J. Catal.* 185, 307 (1999).
98. R. Prasad and S. Vashisht, *J. Chem. Technol. Biotechnol.* 68, 310 (1997).
99. J. M. L. Nieto, P. Concepcion, A. Dejoz, H. Knozinger, F. Melo, and M. I. Vazquez, *J. Catal.* 189, 147 (2000).
100. K. Wada, H. Yamada, E. Watanabe, and T. Mitsudo, *J. Chem. Soc. Faraday Trans.* 94, 1771 (1998).
101. Z. P. Zhu, Z. Y. Liu, S. J. Liu, and H. X. Niu, *Appl. Catal. B Environ.* 23, 229 (1999).
102. H. Bosch, F. J. J. G. Janssen, F. M. G. Van den Kerkhof, J. Oldenziel, J. G. Van Ommen, and J. R. H. Ross, *Appl. Catal.* 25, 239 (1986).
103. M. D. Amiridis, I. E. Wachs, G. Deo, J. M. Jehng, and D. S. Kim, *J. Catal.* 161, 247 (1996).
104. C. R. Dias, M. F. Portgela, M. Galan-Fereres, M. A. Banares, M. L. Granados, M. A. Pena, and J. L. G. Fierro, *Catal. Lett.* 43, 117 (1997).
105. M. G. Nobbenhuis, A. Baiker, P. Barnickel, and A. Wokaun, *Appl. Catal. A General* 85, 157 (1992).
106. M. Sanati, A. Andersson, L. R. Wallenberg, and B. Rebenstorf, *Appl. Catal. A General* 106, 51 (1993).
107. K. V. Narayana, A. Venugopal, K. S. Rama Rao, S. Khaja Masthan, V. V. Rao, and P. Kanta Rao, *Appl. Catal. A General* 167, 11 (1998).
108. F. Cavani, F. Trifiro, P. Jiru, K Habersberger, and W. Tvaruzkova, *Zeolites* 8, 12 (1988).
109. L. J. Burcham, G. T. Gao, X. T. Gao, and I. E. Wachs, *Top. Catal.* 11, 85 (2000).
110. J. P. Dunn, P. R. Koppula, H. G. Stenger, and I. E. Wachs, *Appl. Catal. B Environ.* 19, 103 (1998).
111. J. P. Dunn, H. G. Stenger, and I. E. Wachs, *Catal. Today* 51, 301 (1999).
112. J. P. Dunn, H. G. Stenger, and I. E. Wachs, *J. Catal.* 181, 233 (1999).
113. G. C. Bond, S. Flamerz, and R. Shukri, *Faraday Discuss. Chem. Soc.* 87, 65 (1989).
114. J. Huuhtanen and S. L. T. Andersson, *Appl. Catal. A General* 98, 159 (1993).
115. B. I. Whittington and J. R. Anderson, *J. Phys. Chem.* 97, 1032 (1993).
116. H. H. Patterson, J. Cheng, S. Despres, M. Sunamoto, and M. Anpo, *J. Phys. Chem.* 95, 8813 (1991).
117. S. G. Zhang, S. Higashimoto, H. Yamashita, and M. Anpo, *J. Phys. Chem. B* 102, 5590 (1998).
118. M. A. Banares, L. J. Alemany, M. L. Granados, M. Faraldos, and J. L. G. Fierro, *Catal. Today* 33, 73 (1997).
119. A. Parmaliana, F. Frusteri, A. Mezzapica, M. S. Scurrell, and N. Giordano, *J. Chem. Soc. Chem. Commun.* 751 (1993).
120. R. G. Herman, Q. Sun, C. Shi, K. Klier, C. B. Wang, H. Hu, I. E. Wachs, and M. M. Bhasin, *Catal. Today* 37, 1 (1997).
121. K. T. Li and T. Y. Chien, *Catal. Lett.* 57, 77 (1999).
122. M. J. Bagajewicz, S. S. Tamhankar, M. F. Stephanopoulos, and G. R. Gavalas, *Environ. Sci. Techn.* 22, 467 (1998).
123. B. M. Reddy, E. P. Reddy, and I. Ganesh, *Res. Chem. Intermediat.* 23, 703 (1997).
124. B. M. Reddy, I. Ganesh, and B. Chowdhury, *Chem. Lett.* 1145 (1997).
125. B. M. Reddy, E. P. Reddy, I. Ganesh, and M. V. Kumar, *Ind. J. Chem. Technol.* 4, 256 (1997).

126. F. L. Wang, T. F. Tsai, L. C. Yu, I. Z. Hu, and Y. P. Yen, *Catal. Lett.* 42, 155 (1996).
127. Z. Y. Dang, J. F. Gu, J. Z. Lin, and D. X. Yang, *Chem. Commun.* 1901 (1996).
128. F. L. Wang, L. Yu, W. S. Lee, and W. F. Yang, *J. Chem. Soc. Chem. Commun.* 811 (1994).
129. F. L. Wang, W. S. Lee, Y. F. Liou, and L. C. Chen, *Ind. Eng. Chem. Res.* 32, 30 (1993).
130. F. L. Wang and L. C. Chen, *J. Chem. Soc. Chem. Commun.* 1760 (1991).
131. M. Vassileva, A. Andreev, and S. Dancheva, *Appl. Catal.* 69, 221 (1991).
132. L. Forni and F. Gianetti, *Chim. Ind. Milan* 62, 101 (1980).
133. S. Ishida, S. Imamura, F. Ren, Y. Tatematsu, and Y. Fujimara, *React. Kinet. Catal. Lett.* 46, 199 (1992).
134. P. R. H. P. Rao and A. V. Ramaswamy, *J. Chem. Soc. Chem. Commun.* 1245 (1992).
135. A. Khodakov, B. Olthof, A. T. Bell, and E. Iglesia, *J. Catal.* 181, 205 (1999).
136. K. Chen, A. Khodakov, J. Yang, A. T. Bell, and E. Iglesia, *J. Catal.* 186, 325 (1999).
137. P. Concepcion, J. M. Lopez Nieto, and J. Perez-Pariente, *J. Mol. Catal. A Chem.* 99, 173 (1995).
138. P. R. H. P. Rao, A. V. Ramaswamy, and P. Ratnasamy, *J. Catal.* 137, 225 (1992).
139. M. S. Rigutto and H. van Bekkum, *J. Mol. Catal.* 81, 77 (1993).
140. P. R. H. P. Rao and A. V. Ramaswamy, *Appl. Catal.* 93, 123 (1993).
141. B. M. Weckhuysen, D. Wang, M. P. Rosynek, and J. H. Lunsford, *J. Catal.* 175, 338 (1998).
142. B. M. Weckhuysen, D. Wang, M. P. Rosynek, and J. H. Lunsford, *J. Catal.* 175, 347 (1998).
143. M. P. McDaniel and M. B. Welch, *J. Catal.* 82, 98 (1983).
144. D. L. Myers and J. H. Lunsford, *J. Catal.* 99, 140 (1986).
145. L. R. Mentasy, O. F. Gorriz, and L. E. Cadus, *Ind. Eng. Chem. Res.* 38, 396 (1999).
146. S. De Rossi, G. Ferraris, S. Fremiotti, A. Cimino, and V. Indovina, *Appl. Catal. A General* 81, 113 (1992).
147. A. Hakuli, A. Kytokovi, A. O. I. Krause, and T. Suntola, *J. Catal.* 161, 393 (1996).
148. V. Indovina, *Catal. Today* 41, 95 (1998).
149. V. Indovina, A. Cimino, S. De Rossi, and G. Ferraris, *J. Mol. Catal.* 75, 305 (1992).
150. W. Grunert, W. Saffert, R. Feldhaus, and K. Anders, *J. Catal.* 99, 149 (1986).
151. J. Engweiler, J. Nickl, A. Baiker, K. Kohler, C. W. Schlapfer, and A. van Zelewsky, *J. Catal.* 145, 141 (1994).
152. J. Dong Chen, J. Dakka, E. Neeleman, and R. A. Scheldon, *J. Chem. Soc. Chem. Commun.* 1379 (1993).
153. E. V. Spinace, U. Schuchardt, and D. Cardoso, *Appl. Catal. A General* 185, 193 (1999).
154. D. Wei, N. Yao, and G. L. Haller, *Sci. Technol. Catal.* 35, 239 (1998).
155. N. C. Ramani, D. L. Sullivan, J. G. Eckerdt, J. M. Jehng, and I. E. Wachs, *J. Catal.* 176, 143 (1998).
156. T. Kubo, H. Tominaga, and T. Kunugi, *Bull. Chem. Soc. Jpn.* 46, 3549 (1973).
157. H. Yamashita, M. Ariyuki, S. Higashimoto, S. G. Zhang, J. S. Chang, S. E. Park, J. M. Lee, Y. Masumura, and M. Anpo, *J. Synchrotron Rad.* 6, 453 (1999).
158. S. Kawi and M. Te, *Catal. Today* 44, 101 (1998).
159. A. M. Padilla, J. Corella, and J. M. Toledo, *Appl. Catal. B Environ.* 22, 107 (1999).
160. D. S. Kim and I. E. Wachs, *J. Catal.* 142, 166 (1993).
161. J. H. Uhm, M. Y. Shin, J. Zhidong, and J. S. Chung, *Appl. Catal. B Environ.* 22, 293 (1999).
162. B. Grzybowska, J. Sloczynski, R. Grabowski, K. Wcislo, A. Kozlowska, J. Stoch, and J. Zielinski, *J. Catal.* 178, 687 (1998).
163. J. Santamaria-Gonzalez, J. Merida-Robles, M. Alcantara-Rodriguez, P. Maireles-Torres, E. Rodriguez-Castellon, and A. Jimenez-Lopez, *Catal. Lett.* 64, 209 (2000).
164. J. Dong Chen and R. A. Scheldon, *J. Catal.* 153, 1 (1995).
165. S. B. Wang, K. Murata, T. Hayakawa, S. Hamakawa, and K. Suzuki, *Appl. Catal. A General* 196, 1 (2000).
166. F. L. Wang and T. F. Tsai, *Catal. Today* 44, 259 (1998).
167. D. H. Cho, Y. G. Kim, and J. S. Chung, *Catal. Lett.* 53, 199 (1998).
168. B. M. Weckhuysen, D. Wang, M. P. Rosynek, and J. H. Lunsford, *J. Catal.* 175, 338 (1998).
169. B. M. Weckhuysen, D. Wang, M. P. Rosynek, and J. H. Lunsford, *J. Catal.* 175, 347 (1998).
170. M. A. Baltanas, A. B. Stiles, and J. R. Katzer, *Appl. Catal.* 28, 13 (1986).
171. D. Van der Kleut, Ph.D. Thesis, University of Utrecht, The Netherlands, 1994.
172. M. L. Jacono and M. Schiavello, in "*Preparation of Catalysts*" (B. Delmon, P. A. Jacobs, and G. Poncelet, Eds.), p. 474, Elsevier, Amsterdam, 1976.
173. B. Dhandapani and S. T. Oyama, *Chem. Lett.* 413 (1995).
174. A. Nishino, *Catal. Today* 10, 107 (1991).
175. L. Singoredjo, R. Korver, F. Kapteijn, and J. A. Moulijn, *Appl. Catal. B Environ.* 1, 297 (1992).
176. W. S. Kijlstra, J. C. M. L. Daamen, J. M. Van de Graaf, B. Van der Linden, E. K. Poels, and A. Bliek, *Appl. Catal. B. Environ.* 7, 237 (1996).
177. D. J. Parrillo, C. Pereira, G. T. Kokotailo, and R. J. Gorte, *J. Catal.* 138, 377 (1992).
178. N. Rajic, D. Stojakovic, S. Hocevar, and V. Kaucic, *Zeolites* 13, 384 (1993).
179. W. Li, G. V. Gibbs, and S. T. Oyama, *J. Am. Chem. Soc.* 120, 9041 (1998).
180. W. Li and S. T. Oyama, *J. Am. Chem. Soc.* 120, 9047 (1998).
181. R. Raja, G. Sankar, and J. M. Thomas, *Chem. Commun.* 829 (1999).
182. B. Z. Wan and K. Huang, *Appl. Catal.* 73, 113 (1991).
183. C. Bowers and P. K. Dutta, *J. Catal.* 122, 271 (1990).
184. M. Yonemitsu, Y. Tanaka, and M. Iwamoto, *J. Catal.* 178, 207 (1998).
185. P. P. Knops-Gerrits, D. De Vos, F. Thibault-Starzyk, and P. A. Jacobs, *Nature (London)* 369, 543 (1994).
186. M. F. Luo, X. M. Zheng, and Y. J. Zhong, *Indian J. Chem. A* 38, 703 (1999).
187. M. Marczewski, H. Marczewska, and M. Debowiak, *React. Kinet. Catal. Lett.* 55, 207 (1995).
188. O. V. Krylov, A. K. Mamedov, and S. R. Mirzabekova, *Ind. Eng. Chem. Res.* 34, 474 (1995).
189. V. A. Sadykov and P. G. Tsyrulnikov, *Kinet. Catal.* 18, 113 (1977).
190. V. Duma and D. Honicke, *J. Catal.* 191, 93 (2000).
191. C. T. Wang and R. J. Willey, *Catal. Today* 52, 83 (1999).
192. V. A. Sazonov, Z. R. Ismagilov, and N. A. Prokudina, *Catal. Today* 47, 149 (1999).
193. J. S. Chang, J. Noh, S. E. Park, W. Y. Kim, and C. W. Lee, *Bull. Kor. Chem. Soc.* 19, 1343 (1998).
194. H. Randall, R. Doepper, and A. Renken, *Appl. Catal. B Environ.* 17, 357 (1998).
195. J. S. Chang, S. E. Park, W. Y. Kim, M. Anpo, and H. Yamashita, *Stud. Surf. Sci. Catal.* 114, 387 (1998).
196. C. Pnam-Huu, C. Estournes, B. Heinrich, and M. J. Ledoux, *J. Chem. Soc. Faraday Trans.* 94, 435 (1998).
197. P. H. Cuong, C. Crouzet, C. Estournes, and M. J. Ledoux, *J. Chem. Soc. Faraday Trans.* 94, 443 (1998).
198. H. Randall, R. Doepper, and A. Renken, *Ind. Eng. Chem. Res.* 36, 2996 (1997).
199. L. A. Boot, S. C. van der Linden, A. J. van Dillen, J. W. Geus, and F. R. van Buren, *Rec. Trav. Chim. Pays-Bas* 115, 525 (1996).
200. D. E. Stobbe, F. R. van Buren, A. J. van Dillen, and J. W. Geus, *Stud. Surf. Sci. Catal.* 75, 2337 (1993).

201. Z. H. Suo, Y. Kou, J. Z. Niu, W. Z. Zhang, and H. L. Wang, *Appl. Catal. A General* 148, 301 (1997).
202. K. R. P. M. Rao, F. E. Huggins, V. Mahajan, G. P. Huffman, V. U. S. Rao, B. L. Bhatt, D. B. Bukur, B. H. Davis, and R. J. Obrien, *Top. Catal.* 2, 71 (1995).
203. F. Rodriguez-Reinoso and A. Sepulveda-Escribano, *Appl. Catal.* 77, 95 (1991).
204. R. J. A. M. Terorde, M. C. Dejong, M. J. D. Crombag, P. J. Vandenbrink, A. J. Van Dillen, and J. W. Geus, *Stud. Surf. Sci. Catal.* 82, 861 (1994).
205. X. Feng and W. K. Hall, *J. Catal.* 166, 368 (1997).
206. A. Z. Ma and W. Grunert, *Chem. Commun.* 71 (1999).
207. P. P. Knops-Gerrits, A. Verberckmoes, R. A. Schoonheydt, M. Ichikawa, and P. A. Jacobs, *Micropor. Mesopor. Mater.* 21, 475 (1998).
208. B. M. Weckhuysen, D. Wang, M. P. Rosynek, and J. H. Lunsford, *J. Catal.* 175, 338 (1998).
209. B. M. Weckhuysen, D. Wang, M. P. Rosynek, and J. H. Lunsford, *J. Catal.* 175, 347 (1998).
210. T. Nanba, A. Uemura, A. Ueno, M. Haneda, H. Hamada, N. Kakuta, H. Miura, H. Ohfune, and Y. Udagawa, *Bull. Chem. Soc. Jpn.* 71, 2331 (1998).
211. E. Hayashi, E. Iwamatsu, M. E. Biswas, S. A. Ali, Y. Yamamoto, Y. Yanada, A. K. K. Lee, H. Hamid, and T. Yoneda, *Chem. Lett.* 433 (1997).
212. L. A. Boot, M. H. J. V. Kerkhoffs, B. T. van der Linden, A. J. van Dillen, J. W. Geus, and F. R. van Buren, *Appl. Catal. A General* 137, 69 (1996).
213. A. S. K. Sinha and V. Shankar, *Chem. Eng. J. Biochem. Eng. J.* 52, 115 (1993).
214. J. A. Dalmon, P. Chaumette, and C. Mirodatos, *Catal. Today* 15, 101 (1992).
215. A. A. Adesin, R. R. Hudgins, and P. L. Silveston, *React. Kinet. Catal. Lett.* 37, 157 (1998).
216. S. Hocevar, J. Batista, and V. Kaucic, *J. Catal.* 139, 351 (1993).
217. B. Kraushaar-Czarnetzki, W. G. M. Hoogervorst, and W. H. J. Stork, *Stud. Surf. Sci. Catal.* 84, 1869 (1994).
218. H. F. W. J. van Breukelen, M. E. Gerritsen, V. M. Ummels, J. S. Broens, and J. H. C. van Hooff, *Stud. Surf. Sci. Catal.* 105, 1029 (1997).
219. J. Meusinger, H. Vinek, G. Dworeckow, M. Goepper, and J. A. Lercher, *Stud. Surf. Sci. Catal.* 69, 373 (1991).
220. D. L. Vanoppen, D. E. De Vos, M. J. Genet, P. G. Rouxhet, and P. A. Jacobs, *Angew. Chem. Int. Ed. Engl.* 34, 560 (1995).
221. M. Hartmann, A. Poppl, and L. Kevan, *Stud. Surf. Sci. Catal.* 101, 801 (1996).
222. V. Mavrodinova, Y. Neinska, C. Minchev, H. Lechert, V. Minkov, V. Valtchev, and V. Penchev, in "Zeolite Chemistry, and Catalysis" (P. A. Jacobs et al., Eds.), Elsevier Science Publishers, Amsterdam, 1991.
223. I. V. Babich, Y. V. Plyoto, A. D. Van Langeveld, and J. A. Moulijn, *Appl. Surf. Sci. 115*, 267 (1997).
224. L. P. Lindfors and S. Smedts, *Catal. Lett.* 27, 323 (1994).
225. P. Moriceau, B. Grzybowska, and Y. Barbaux, *Pol. J. Chem.* 72, 910 (1998).
226. R. Spinicci and A. Tofanari, *Mater. Chem. Phys.* 25, 375 (1990).
227. A. Sayari, A. Ghorbel, G. M. Pajonk, and S. J. Teichner, *React. Kinet. Catal. Lett.* 15, 459 (1980).
228. M. Iwamato and H. Yahiro, *Catal. Today* 22, 5 (1994).
229. B. M. Weckhuysen, A. A. Verberckmoes, I. P. Vannijvel, P. L. Buskens, P. A. Jacobs, and R. A. Schoonheydt, *Angew. Chem. Int. Ed. Engl.* 34, 2652 (1995).
230. Z. M. Wang and Y. S. Lin, *Ind. Eng. Chem. Res.* 37, 4675 (1998).
231. M. F. Luo and X. N. Zheng, Acta *Chem. Scand.* 52, 1183 (1998).
232. P. Artizzu, E. Garbowski, M. Primet, Y. Brulle, and J. Saint-Just, *Catal. Today* 47, 83 (1999).
233. Z. P. Zhu, Z. Y. Liu, S. J. Liu, H. X. Niu, T. D. Hu, T. Liu, and Y. N. Xie, *Appl. Catal. B Environm.* 26, 25 (2000).
234. P. O. Larsson, A. Andersson, L. R. Wallenberg, and B. Svensson *J. Catal.* 163, 279 (1996).
235. A. M. Youssef, L. B. Khalil, A. A. Attia, and T. Elnabarawy, *Mater Lett.* 24, 253 (1995).
236. A. Fortuny, C. Ferrer, C. Bengoa, J. Font, and A. Fabregat, *Catal Today* 24, 79 (1995).
237. H. Rajesh and U. S. Ozkan, *Ind. Eng. Chem. Res.* 32, 1622 (1993).
238. G. J. Millar, C. H. Rochester, and K. C. Waugh, *Catal. Lett.* 14, 285 (1992).
239. C. Rocchiccioli-Deltcheff, M. Amirouche, M. Che, J. M. Tatibouet, and M. Fournier, *J. Catal.* 125, 292 (1990).
240. W. Zang and S. T. Oyama, *J. Phys. Chem.* 100, 10759 (1996).
241. D. S. Kim, I. E. Wachs, and K. Segawa, *J. Catal.* 146, 268 (1994).
242. Y. Kikutani, *J. Mol. Catal. A Chemical* 142, 265 (1999).
243. J. Abart, E. Delgado, G. Est, H. Jeziorowski, H. Knozinger, N. Thille, X. Z. Wang, and E. Taglauer, *Appl. Catal.* 2, 155 (1982).
244. T. Ono, M. Anpo, and Y. Kubokawa, *J. Phys. Chem.* 90, 4780 (1986).
245. Y. I. Yermakov, *Catal. Rev.* 14, 78 (1976).
246. L. Wang, L. Tao, M. Xie, and G. Xu, *Catal. Lett.* 21, 35 (1993).
247. F. Solymosi, A. Erdohelyi, and A. Szoke, *Catal. Lett.* 32, 43 (1995).
248. D. Wang, J. H. Lunsford, and M. P. Rosynek, *Top. Catal.* 3, 289 (1996).
249. H. Bosch and F. Janssen, *Catal. Today* 2, 369 (1988).
250. J. M. Stencil, J. R. Diehl, J. R. D'Este, L. E. Makovsky, L. Rodrigo, K. Marchinkowska, A. Adnot, P. C. Roberge, and S. Kaliaguine, *J. Phys. Chem.* 90, 4739 (1986).
251. R. Pearce, in "Catalysis" (C. Kemball and D. A. Dowden, Eds.), Vol. 2, p. 183. Chemical Society, London, 1978.
252. Y. C. Park and H. K. Rhee, *Appl. Catal. A General* 179, 145 (1999).
253. M. C. Tsai, Y. W. Chen, B. C. Kang, J. C. Wu, and L. J. Leu, *Ind. Eng. Chem. Res.* 30, 1801 (1991).
254. N. C. Ramani, D. L. Sullivan, and J. G. Ekerdt, *J. Catal.* 173, 105 (1998).
255. K. D. Chen, S. B. Xie, E. Iglesia, and A. T. Bell, *J. Catal.* 189, 421 (2000).
256. V. Logie, P. Wehrer, A. Katrib, and G. Maire, *J. Catal.* 189, 438 (2000).
257. S. T. Oyama, W. Li, and W. M. Zhang, *Stud. Surf. Sci. Catal.* 121, 105 (1999).
258. A. S. C. Brown, H. J. Hargreaves, and S. H. Taylor, *Catal. Lett.* 57, 109 (1999).
259. F. Arena, N. Giordano, and A. Parmaliana, *J. Catal.* 167, 66 (1997).
260. I. Peeters, A. W. D. van der Gon, M. A. Reijme, P. J. Kooyman, A. M. de Jong, J. van Grondelle, H. H. Brongersma, and R. A. van Santen, *J. Catal.* 173, 28 (1998).
261. A. Erdohelyi, F. Mate, and F. Solymosi, *Catal. Lett.* 8, 229 (1991).
262. A. N. Desikan, W. M. Zhang, and S. T. Oyama, *J. Catal.* 157, 740 (1995).
263. A. Debal, G. Rafaralahitsimba, and E. Ucciani, *Fett. Wiss. Technol.* 95, 236 (1993).
264. R. V. Morris, D. R. Maywell, and J. W. Sheppard, *J. Less-Common Met.* 36, 395 (1974).
265. Z. Zhang, J. Suo, X. Zhang, and S. Li, *Appl. Catal. A General* 179, 11 (1999).
266. Z. Zhang, J. Suo, X. Zhang, and S. Li, *Chem. Commun.* 241 (1998).
267. K. Weissermal and H. J. Arpe, "Industrial Organic Chemistry," Verlag Chemie, New York, 1978.
268. A. De Lucas, J. L. Valverde, P. Canizares, and L. Rodriguez, *Appl. Catal. A General* 184, 143 (1999).
269. V. M. Benitez, C. A. Querini, N. S. Figoli, and R. A. Comelli, *Appl. Catal. A General* 178, 205 (1999).
270. J. L. Zeng, Z. T. Xiong, H. B. Zhang, G. D. Lin, and K. R. Tsai, *Catal. Lett.* 53, 119 (1998).
271. H. Bosch and F. Janssen, *Catal. Today* 2, 369 (1988).
272. T. Yamaguchi, S. Nakamura, and K. Tanabe, *J. Chem. Soc. Chem. Commun.* 621 (1982).
273. G. J. Hutchings, J. L. van Rensburg, W. Pickl, and R. Hunter, *J. Chem. Soc. Faraday Trans.* 84, 1311 (1988).

274. J. Ramirez, S. Fuentes, G. Diaz, M. Vrinat, M. Breysse, and M. Lacroix, *Appl. Catal.* 52, 211 (1989).
275. M. Hino and K. Arata, *J. Chem. Soc. Chem. Commun.* 1259 (1987).
276. J. G. Wu and S. B. Li, *J. Phys. Chem.* 99, 4566 (1995).
277. J. A. Moulijn, C. Boelhouw, and H. J. Reitsma, *J. Catal.* 25, 434 (1995).
278. T. Yamaguchi, S. Nakamura, and K. Tanabe, *J. Chem. Soc. Chem. Commun.* 621 (1982).
279. J. C. Mol, *Catal. Today* 51, 299 (1999).
280. I. E. Wachs, G. Deo, A. Andreini, M. A. Vuurman, and M. de Boer, *J. Catal.* 160, 322 (1996).
281. Z. Zhu and J. H. Espenson, *J. Mol. Catal. A Chemical* 121, 139 (1997).
282. I. E. Wachs, G. Deo, D. S. Kim, M. A. Vuurman, and H. Hu, *J. Mol. Catal.* 83, 443 (1993).
283. P. S. Kirlin and B. C. Gates, *Nature (London)* 325, 38 (1987).
284. A. W. Aldag, C. J. Lin, and A. Clark, *J. Catal.* 51, 278 (1978).
285. I. E. Wachs, *Proc. Int. Conf. Niobium Tantalum* 679 (1989).
286. J. M. Jehng and I. E. Wachs, *High. Temp. Mater. Proc.* 11, 159 (1993).
287. T. Tanaka, S. Takenaka, T. Funabiki, and S. Yoshida, *Chem. Lett.* 809 (1994).
288. J. M. Jehng, A. M. Turek, and I. E. Wachs, *Appl. Catal. A General* 83, 179 (1992).
289. S. Okazaki and T. Okuyama, *Bull. Chem. Soc. Jpn.* 56, 2159 (1983).
290. J. M. Jehng and I. E. Wachs, *Catal. Today* 8, 37 (1990).
291. J. M. Jehng and I. E. Wachs, *Catal. Today* 16, 417 (1993).
292. I. E. Wachs, J. M. Jehng, G. Deo, H. Hu, and N. Arora, *Catal. Today* 28, 199 (1996).
293. N. Ichikuni, M. Shirai, and Y. Iwasawa, *Catal. Today* 28, 49 (1996).
294. T. Tanaka, S. Takenaka, T. Funabiki, and S. Yoshida, *Chem. Lett.* 4, 809 (1994).
295. P. Moggi and G. Albanesi, *Appl. Catal.* 68, 285 (1991).
296. J. H. Lunsford, *Angew. Chem. Int. Ed. Engl.* 107, 1059 (1995).
297. S. C. Tsang, J. B. Claridge, and M. L. H. Green, *Catal. Today* 23, 3 (1995).
298. M. Faraldos, M. Banares, J. A. Anderson, H. Hu, I. E. Wachs, and J. L. G. Fiero, *J. Catal.* 160, 214 (1996).
299. O. V. Bragin, T. V. Vasina, A. V. Preobrazhenskii, and K. M. Minaches, *Izv. Akad. Nauk SSSR, Ser. Khim.* 3, 750 (1989).
300. T. V. Vasina, A. V. Preobrzshenskii, S. A. Isaev, O. V. Chetina, O. V. Masloboishikova, and O. V. Bragin, *Kinet. Catal.* 35, 93 (1994).
301. L. Wang, L. Tao, M. Xie, J. Huang, and Y. Xu, *Catal. Lett.* 21, 35 (1993).
302. Y. Xu, S. Liu, L. Wang, M. Xie, and X. Guo, *Catal. Lett.* 30, 135 (1995).
303. L. Chen, L. Lin, Z. Xu, X. Li, and L. Tao, *Stud. Surf. Sci. Catal.* 94, 495 (1995).
304. Y. Xu, Y. Shu, S. Liu, J. Huang, and X. Guo, *Catal. Lett.* 35, 233 (1995).
305. S. Wong, Y. Xu, L. Wang, S. Liu, G. Li, M. Xie, and X. Guo, *Catal. Lett.* 38, 39 (1996).
306. Y. Xu, W. Liu, S. Wong, L. Wang, and X. Guo, *Catal. Lett.* 40, 207 (1996).
307. D. Wang, M. P. Rosynek, and J. H. Lunsford, *Top. Catal.* 3, 289 (1996).
308. D. Wang, J. H. Lunsford, and M. P. Rosynek, *J. Catal.* 169, 347 (1997).
309. F. Solymosi, E. Erdohelyi, and A. Szoke, *Catal. Lett.* 32, 43 (1995).
310. F. Solymosi, A. Szoke, and J. Cserenyi, *Catal. Lett.* 19, 157 (1996).
311. A. Szoke and F. Solymosi, *Appl. Catal.* 142, 361 (1996).
312. F. Solymosi, J. Cserenyi, A. Szoke, T. Bansagi, and A. Oszko, *J. Catal.* 165, 150 (1997).
313. J. Z. Zhang, M. A. Long, and R. F. Howe, *Catal. Today* 44, 293 (1998).
314. B. M. Weckhuysen, M. P. Rosynek, and J. H. Lunsford, *Catal. Lett.* 52, 31 (1998).
315. B. M. Weckhuysen, D. Wang, M. P. Rosynek, and J. H. Lunsford, "Proceedings of the 12th International Zeolite Conference," p. 1381 (M. M. J. Treacy, B. K. Marcus, M. E. Bisher, and J. B. Higgins, Eds.), Materials Reseach Society, Warrendale, PA, 1999.
316. C. T. Kresge, M. E. Leonowicz, W. J. Roth, J. C. Vartuli, and J. S. Beck, *Nature (London)* 359, 710 (1992).
317. J. S. Beck, J. C. Vartuli, W. J. Roth, M. E. Leonowicz, C. T. Kresge, K. D. Schmitt, C. T. W. Chu, D. H. Olson, E. W. Sheppard, S. B. McCullen, J. B. Higgins, and J. L, Schlenker, *J. Am. Chem. Soc.* 114, 10834 (1992).
318. T. Maschmeyer, F. Rey, G. Sankar, and J. M. Thomas, *Nature (London)* 378, 159 (1995).
319. M. Yonemitsu, Y. Tanaka, and M. Iwamoto, *Chem. Mater.* 9, 2679 (1997).
320. M. Yonemitsu, Y. Tanaka, and M. Iwamoto, *J. Catal.* 178, 207 (1998).
321. R. R. Rao, B. M. Weckhuysen, and R. A. Schoonheydt, *Chem. Commun.* 445 (1999).
322. B. M. Weckhuysen, R. R. Rao, J. Pelgrims, R. A. Schoonheydt, P. Bodart, G. Debras, O. Collart, P. Van Der Voort, and E. F. Vansant, *Chem. Eur. J.* 6, 2960 (2000).
323. F. Buonomo, D. Sanfilippo, and F. Trifiro, in "Handbook of Heterogeneous Catalysis" (G. Ertl, H. Knozinger, and J. Weitkamp, Eds.), p. 2140. Wiley-VCH, Weinheim, 1997.
324. B. M. Weckhuysen, A. A. Verberckmoes, J. Debaere, K. Ooms, I. Langhans, and R. A. Schoonheydt, *J. Mol. Catal. A Chemical* 151, 115 (2000).
325. B. M. Weckhuysen, A. Bensalem, and R. A. Schoonheydt, *J. Chem. Soc. Faraday Trans.* 94, 2011 (1998).
326. S. De Rossi, G. Ferraris, S. Fremiotti, A. Cimino, and V. Indovina, *Appl. Catal. A General* 81, 113 (1992).
327. A. Amirnazmi, J. E. Benson, and M. Boudart, *J. Catal.* 30, 55 (1973).
328. Y. J. Li and J. N. Armor, *Appl. Catal.* 1, 21 (1992).
329. Y. Li and W. K. Hall, *J. Catal.* 129, 202 (1991).
330. M. Iwamoto, H. Furukawa, Y. Mine, F. Uemura, S. Mikuriya, and S. Kagawa, *J. Chem. Soc. Chem. Commun.* 1272 (1986).
331. M. Iwamoto, H. Yahiro, K. Tanda, N. Mizuno, Y. Mine, and S. Kagawa, *J. Phys. Chem.* 95, 3727 (1991).
332. M. Iwamoto, H. Yahiro, N. Mizuno, W. Zhang, Y. Mine, H. Furukawa, and S. Kagawa, *J. Phys. Chem.* 96, 9360 (1992).
333. J. Valyon and W. K. Hall, *J. Catal.* 143, 520 (1993).
334. M. Iwamoto, S. Yokoo, K. Sakai, and S. Kagawa, *J. Chem. Soc. Faraday Trans.* 77, 1629 (1981).
335. M. Iwamoto, H. Yahiro, Y. Mine, and S. Kagawa, *Chem. Lett.* 213 (1989).
336. W. F. Schneider, K. C. Hass, R. Ramprasad, and J. B. Adams, *J. Phys. Chem. B* 102, 3692 (1998).
337. E. Giamello, D. Murphy, C. Magnacca, C. Morterra, Y. Shioya, T. Nomura, and M. Anpo, *J. Catal.* 136, 510 (1992).